

SSC
EOI
0002

May 23, 1990

Library
Use
Only

LOW P_c PHYSICS AT THE SSC
an Expression of Interest

SSCL-SR-1157
SSC-EOI0002

Contact person: Jay Orear, Cornell University

M. Bertani, S. Zucchelli - University of Bologna; A. Garren - University of California, Berkeley; R. DeSalvo - CERN; R. Mondardini, J. Orear - Cornell University; N. Amos, W. Baker, N. Gelfand, S. Pruss, R. Rubinstein, S. Shukla - Fermilab; A. Breakstone - University of Hawaii; L. Jones, M. Longo - University of Michigan; M. Block - Northwestern University; K. Goulianos, A. Vacchi - Rockefeller University; D. Johnson - SSC Laboratory; C. Guss - Temple University

ABSTRACT

Experimental systems and detectors are proposed which can measure (1) small angle elastic scattering into the coulomb region, (2) large angle elastic scattering, (3) single diffraction dissociation, and (4) other small angle processes which would be missed by a typical 4π detector. The small angle elastic scattering is used via the optical theorem to obtain σ_c and the ρ -value. (See Part A.) Requirements on accelerator design are discussed. Beta at the interaction point must be ~ 2 km in order to do the small angle elastic scattering. Such high beta is not needed at the detector positions. The intermediate beta region is well suited for the large angle elastic scattering and the single diffraction scattering. (See Part B.)

PART A

I. Elastic Scattering

The physics goal is to find out just how fast σ_c is rising and what is the precise shape of its energy dependence. Also, is elastic scattering which is expected to be pure imaginary at high energy becoming real instead; i.e., is the ρ -value still increasing? (UA4 claims it has reached 0.25 at $\sqrt{s} = 0.546$ TeV. With such a high ρ -value, dispersion relations predict an even more rapid rise in σ_c at energies above the SPS - especially for pp as compared to $p\bar{p}$.) Just how fast is the mean squared radius (as measured by the slope parameter B) increasing? Is the proton becoming more black? Is the forward diffraction peak curving toward the t-axis rather than away? Are there diffraction minima? If so, how many? In order to answer all these questions, short runs at several energies such as $\sqrt{s} = 2, 5, 10, 20, 40$ TeV would be useful. Fig. 1 shows that the pp total cross section is expected to be ~ 120 mb at $\sqrt{s} = 40$ TeV. (1) Fig. 1 shows recent results obtained by E710 at Fermilab. (2) This same technique (with improvements) is proposed for use at the SSC by some of the same experimenters. (2)

In order to measure the ρ -value and to use the coulomb amplitude for normalization of $d\sigma/dt$ it is necessary to get to scattering angles smaller than $1.2 \mu\text{rad}$. At this angle the coulomb amplitude equals the nuclear amplitude when $\sqrt{s} = 40$ TeV and $\sigma_c = 125$ mb. We set our goal $\theta_{\text{min}} = 0.8 \mu\text{rad}$ where the coulomb cross section would be 5 times the nuclear cross section. Such a small angle is smaller than the typical angular divergence of the beam which is

$$\Delta\theta_y = \sqrt{\epsilon_y/\beta_y^*} \tag{1}$$

where ϵ_y is the vertical emittance and β^* is the beta function at the interaction. The emittance ϵ_y is defined as $\epsilon_y = \sigma_y^2/\beta_y$. Using this definition ϵ_y is 15% of the (y, y') phase space. The normalized emittance

$\epsilon_n = \gamma \epsilon$ is planned to be 10^{-6} m for the SSC, but after appropriate beam scraping it is expected to be 5×10^{-7} m.

a. Determination of β at the interaction point

We set our goal for beam divergence $\Delta\theta_y = 0.14 \theta_{\min}$ which is 0.11 μrad . Solving for β^* in Eq. 1 gives $\beta^* = \epsilon / \Delta\theta^2 = 2000$ m using $\epsilon = 0.5/\gamma$ mm- μrad for the emittance as defined above. By using such a high β one can force the beam divergence to be small enough, but then the source spot size σ_y gets unusually large; i.e., 225 μm . This is not a problem if the detector is placed at a position where the spot size is small and the beam divergence correspondingly larger. (The detector measures position rather than angle. See next paragraph.)

b. Beams at the detectors

The usual detection scheme is to use a high resolution particle detector for each of the scattered protons. (See Fig. 2). The detectors are pushed close to the beam after it is in a clean, stored condition. The size of the spot at the IP (interaction point) cancels out if one can achieve a parallel to point focussing condition. This is achievable at those detector positions where

$$\cot \psi_1 = -\alpha^* \tag{2}$$

(ψ_1 is the phase advance from the IP to detector 1.)

At those positions where Eq. 2 is true, the bracketed quantity in the following relation will be zero and y will be independent of the spot size y_0 .

$$y = \sqrt{(\beta/\beta^*)} (\cos \psi + \alpha^* \sin \psi) y_0 + \sqrt{(\beta\beta^*)} \sin \psi y_0' \tag{3}$$

We shall see in Section II that $\alpha^* = 0$, hence the condition for eliminating the effects of spot size is to locate the detectors at regions of phase advance which are near odd multiples of $\pi/2$.

We define effective length $L = y/y_0'$ where y_0' is the vertical scattering angle and y is the vertical distance from the beam at the detector.

We see from Eq.3 that the effective length is

$$L = \sqrt{(\beta\beta^*)} \sin \psi$$

The lattice solution described in Sec. II has $\beta_1 = 700$ m and $\psi_1 = 3\pi/2$ in x and $5\pi/2$ in y . Then the effective length is ~ 1200 m and the closest distance to the beam will be $y_{\min} = 0.95$ mm. The beam spot size at the detector position is

$$\sigma_y = \sqrt{(\beta_1 z)} = 132 \text{ } \mu\text{m};$$

i.e., the detector is 7 standard deviations from the beam. It is important that this 0.95 mm space from the beam not contain any significant material such as a detector wall. As shown in Sec. IV, this space can be kept free of material. We shall see in the next paragraph that there is no need to have a measuring resolution greater than the spot size; i.e., a detector resolution $\sim 100 \text{ } \mu\text{m}$ or less is fine. So as long as the detector can meet these conditions there is no need for high beta at the detector position. The detector described in Section IV has a measuring resolution of $\sim 30 \text{ } \mu\text{m}$.

c. Measurement resolution

Now we shall calculate the intrinsic accuracy of the angle measurement and show how it is independent of β at the detector. We shall call $y_m' = y_1/L$ the measured vertical scattering angle. Dividing both sides of Eq. 3 by L gives

$$y_m' = y_0' + (\cot \psi_1 + \alpha^*) y_0/\beta^* \tag{4}$$

where y_0 is y -position of the scattering and y_0' is its angle. If the detector position meets the condition of Eq. 2, $y_m' = y_0'$ independent of y_0 . Then $(y_m')_{\text{rms}} = (y_0')_{\text{rms}}$ which is the beam angle spread at the IP. This equals $\sqrt{(\epsilon/\beta^*)} = 0.11 \text{ } \mu\text{rad}$ for $\beta = 2$ km. This can be reduced by the factor $\sqrt{2}$ by averaging measured angles on both sides of the IP.

The detector measuring resolution need be no better than $L (y_m')_{rms} = \sqrt{\beta z}$ which is the same as the spot size at the detector position. With infinitely accurate detectors, the scattering angle can be determined to an accuracy of $.08 \mu\text{rad}$ which is about 10% of the minimum angle to be measured.

We conclude that no matter how high energy is the accelerator, and no matter how poor is the emittance, it is theoretically possible to measure in the coulomb region as long as one has high enough β at the interaction point. The intrinsic angular resolution at the detector position is independent of the local β and is best if the phase advance is near an odd multiple of 90° . The main disadvantage of small β at the detector is that the distances to be measured become small. Certainly the distances should be made significantly larger than the wall thickness and the measuring accuracy of the detector.

d. Normalization

If one is to determine σ_c to $\sim 1\%$ accuracy, one must know the luminosity to a similar or better accuracy. There are two methods where such accuracy can be achieved: (1) the Coulomb Method, and (2) the Combined Method.

(1) the Coulomb method

Since the coulomb amplitude is precisely known and becomes much larger than the nuclear amplitude at very small angles, measurements of dN/dt in the coulomb region thus determine the integrated luminosity. The very same data in the larger angle region then give the nuclear amplitude, which when extrapolated to zero gives the product $(1 + \rho^2) \sigma_c^2$ via the optical theorem:

$$\left. \frac{d\sigma_n}{dt} \right|_0 = \frac{1+\rho^2}{16\pi} \sigma_c^2 \quad (5)$$

It should be easier to reach the coulomb region when running at lower energies (for the same value of y at the detector, the t -value goes as E^2 where E is the beam energy). For this and other reasons it is important to run at several different energies.

An accurate luminosity monitor could be established by mounting two counters on opposite sides of the IP. the coincidence rate would be proportional to the luminosity (which is obtained from the number of deep coulomb events). The same configuration of 2 counters could be used in any other interaction region for continuous readout of luminosity.

(2) the combined method

In case one is not able to get deep into the coulomb region, the Combined Method offers a fall-back position. To use this method, one must monitor the total number of interactions at the same time one is measuring dN_{e1}/dt . Eq. 5 shows that the latter is proportional to luminosity times $(1 + \rho^2) \sigma_c^2$. The total number of interactions ($N_{e1} + N_{inel}$) is proportional to luminosity times σ_c . In taking the ratio the luminosity cancels out leaving the product $(1 + \rho^2)\sigma_c$. This method is best done in a medium- β IR by using a series of "concentric" ring counters on both sides of the IP and extrapolating to zero. dN_{e1}/dt would be well measured at $-t = 3 \times 10^{-3} \text{ GeV}^2$ as explained in Sect. III. It could be extrapolated to zero by normalizing the high- β results to the medium- β data. Then one would have both N_{inel} and $(dN_{e1}/dt)_{t=0}$ for the medium- β IR. The ratio

$$\frac{(dN_{e1}/dt)_0}{N_{e1} + N_{inel}} = \frac{(1 + \rho^2)\sigma_c^2}{16\pi} \tag{6}$$

Another reason for measuring N_{inel} at medium β rather than high β is that $N_{inel} = (N_{double} + 2N_{single})$ where N_{double} is the number of "left-right" coincidences, whereas N_{single} is the number of single arm events in either arm. We estimate that for luminosity $> 10^{31} \text{ cm}^{-2}\text{s}^{-1}$ the beam-gas background will be less than the single arm event rate.

It should be noted that the slope parameter B and the ρ -value can be determined without any knowledge of the luminosity. Fig. 3 shows a set of dN_{e1}/dt curves all normalized to one at $\theta = 10 \mu\text{rad}$. They all have the same slope of $B = 20 \text{ GeV}^{-2}$, but differing values of ρ . A run with ~ 1000 events in the region $2 < \theta < 3 \mu\text{rad}$ could determine ρ even if the data did not reach angles smaller than $2 \mu\text{rad}$.

e. Event rate and running conditions

Let R be the number of elastic events detected per second. Then

$$R = (d\sigma/dt)\Delta t\Delta\phi/2\pi$$

Assume L is 1% of its design value; i.e. $L = 10^{31} \text{ cm}^{-2}\text{s}^{-1}$ for $\beta^* = .5\text{m}$. Then $L = 2.5 \times 10^{27}$ for $\beta^* = 2 \text{ km}$. Using $d\sigma/dt = 10^{-24} \text{ cm}^2/\text{GeV}^2$, $\Delta t = .04 \text{ GeV}^2$, and $\Delta\phi/2\pi = 0.5$ gives $R = 50$ events per second not including the coulomb part of the cross section. This is 18×10^4 per hour. We see that at very low luminosities the running time to get good statistics is almost insignificant.

It is very important to minimize beam halo. Experience with E710 at Fermilab has shown that "deep" scraping down into the outer parts of the beam itself with a final horizontal scrape at inside radius gave the cleanest conditions along with a significant reduction in emittance (up to a factor of 5 at the Tevatron). Rescraping every hour or so might be necessary. Bunch spacing would be increased to eliminate the problem of premature bunch overlaps on either side of the IP. Experience has shown that the best results are obtained during a short, dedicated run. Detector shake-down and tune-up can be done when other experiments have control of the beam.

f. Background rates

The detector described in Sect. IV is read out by an existing CCD with a readout time of $\sim 5 \text{ ms}$. The purpose of this paragraph is to demonstrate

that even with a readout this slow, the experiment is easily do-able without having to rely on any newer, faster technology such as multi-channel phototubes (about 3000 channels would be needed). The existing Thompson CCD chips have a side-by-side buffer. The first "image" to reach the CCD is quickly shifted into the buffer. If two "images" reach the CCD within 5 ms the image intensifier must be gated off until readout of the first is completed. In order to give some idea of deadtime as a function of background rate, we shall give some specific examples.

Suppose the bunch spacing is set to 100 ns. Then a halo singles rate in each detector of 35 kHz gives a left-right accidental rate of 250 Hz. Fortunately the CCD can be cleared in $-1 \mu\text{s}$ and would be cleared if a LR coincidence did not arrive within the time ($4\mu\text{s}$) it takes to form and deliver the LR coincidence. In order to avoid pile-up of more than one track, each image intensifier is gated off for $4 \mu\text{s}$ just after its trigger counter registers a hit. (The probability of 2 hits being registered at these rates would then be 0.003 for a single detector.) The singles rate of 35 kHz times $4 \mu\text{s}$ gives a dead time of 14% due to singles for each detector. The overall acquisition rate would then be -144 halo-halo accidentals per second (overall deadtime of 42%). For comparison, a singles rate of 20 kHz gives 80 halo-halo accidentals per second and an acquisition rate of 63 per sec or a 21% deadtime. If the elastic events were -2 per sec in the presence of -250 per sec background, the intrinsic measuring resolution of $-130 \mu\text{m}$ results in a background rejection factor greater than 100. Clearly the experiment is do-able with an event rate of 2 per sec in the presence of a background accidental rate 100 times larger. The deadtime rapidly becomes smaller for lower singles rates.

In E710 the detectors were able to get 2 mm from the beam where a singles rate -5 kHz was observed. In this experiment we want to get twice as close, but the emittance will be -10 times smaller and we can tolerate -10 times more singles rate. Things may not be 10×10 times easier at the SSC compared to the Fermilab situation, but it looks like we more than enough safety factors here.

II. How to obtain high β

David Johnson has obtained a high β design which meets all of the above conditions. (See Fig. 4.) It is a modification of one of the "intermediate- β " interaction regions. It would be "in series" with another intermediate- β interaction region. This insert has no adverse effect on operation of the accelerator. The provision for doing this kind of physics should be designed into the machine from the very beginning. It would be wise to dedicate one of the four initial IR's to this physics from the beginning since early operation is necessarily at low luminosity and this physics does not require high luminosity. Each detector takes only a few centimeters of linear space; however, the detectors are room temperature inserts in what would otherwise be a cold beam pipe. These helium bypass regions should be constructed from the beginning.

The detector locations are -580 m from the IP with vertical bends but no horizontal bends. For this reason the detectors would be mounted horizontally. After a clean, scraped beam is achieved they would be moved in x to a position -1mm from the beam.

The physics described in Part B could be done in the adjoining medium- β straight. That IR could be instrumented with a track detector for the high mass "decays". One of our detectors would be placed in the region of bend between the two long straight section where η_x gets as large as 1.4 m. The detectors in the high β straight could also be used as part of the single diffractive spectrometer. The spectrometer would cover $M^2/s < 0.015$

The higher mass region would only use the vertical bend where η_y gets as large as 0.3 m. Then $M^2/s - 0.07$ could be reached.

III. Large angle elastic scattering

It is of interest to obtain the shape of the "diffraction" pattern. At Fermilab and ISR energies, there is the prominent $t = 1.4$ dip, but no sign of a second dip. At $\sqrt{s} = 540$ GeV this dip has become a sharp kink at $t = 0.9$ GeV². At the SSC it should move down to -0.37 GeV², and if the proton is becoming blacker as expected, the second dip should show up at -1.5 GeV². (See Fig. 5.) Assuming 10 mm high detectors 0.8 mm from the beam and $L_{eff} = 1000$ m, the t -range is .00025 to .04 GeV². The same apparatus can be used to measure large angle scattering if the colliding region can be reconfigured from high beta to lower beta. If β^* can be reduced from 2000 m to 50 m, the t -range would be from .01 to 1.6 GeV². This should give good coverage of the first two dips. As is discussed in Part B, single diffractive and other small angle processes are best studied in one of the medium β interaction regions which are to be tuneable from $\beta = 10$ to 60 m. For $\beta^* = 30$ m the region covered is $.013 < -t < 3.5$ GeV². This would straddle the first three dips.

IV. Detector design

A group consisting of some experimenters from Fermilab E710 is presently designing and constructing a new kind of detector which can get closer to the beam and give an order of magnitude improvement in spatial resolution. They hope to have a prototype completed in time for running in the next colliding beam run at Fermilab. Such running will provide testing of an SSC prototype as well as obtaining the ρ -value and an improved measurement of the total cross section at the full Tevatron energy.

The new detector is shown schematically in Fig. 6 (the SSC version would be similar, but smaller). The scattered particle travels 3 cm lengthwise along a bundle of 200 μ m scintillating fibers. Light from these fibers is transported by fiber optics to a two stage multichannel image intensifier unit which is read out by a CCD. All the components are commercially available. At the Tevatron, the existing Roman pot top plates and bellows would be used.

In order to avoid any outgassing problem, the fiber bundles would be encapsulated by a 0.2 μm thick layer of sputtered nickel.

Radiation damage is no problem. The detectors will be automatically retracted whenever the singles rate exceeds 100 kHz. They would be physically removed during initial tuneup of the accelerator. At most the average radiation rate would be 5×10^4 particles/cm²/s. One full year at this continuous level corresponds to a radiation exposure of 4×10^5 rads. This is many orders of magnitude below the level which gives noticeable radiation damage to plastic scintillator. This is confirmed by the experience of E710 at the Tevatron.

The estimated cost of each SSC detector is -50KS (exclusive of the moving mechanism). A complete system of 4 such detectors for elastic scattering at the positions shown in Fig. 4 including moving mechanism would cost -\\$300,000 for parts and machining.

The first MCP (multichannel plate) could be gated on only during the bunch passage time. If the singles rate is 50 kHz (see Sec. If), the 20% probability of 2 particles in one detector could be reduced to 0.5% by turning off the MCP for 4 μs each time a single is registered in the trigger counter. After the 4 μs wait for a left-right coincidence, normal operation of the MCP's is resumed and the CCD is cleared.

V. Milestones

The first prototype has been designed and is now under construction at CERN. It should be ready for installation in the Tevatron by Summer 1991. We hope to take data during a dedicated elastic run in late 1992. Final design of the SSC detector should be completed in 1993. Construction and testing in 1994. Insertions in SSC tunnel in 1995. (Detectors would be removed during initial tune-up of SSC beams.)

At present any high energy physicist who shows interest and requests to be listed in this EOI is accepted. Later, standards for institutional

support and personal time commitments will be worked out. So far, 13 out of the 20 names are experimenters connected with E710 at the Tevatron.

Part A References

- (1) M. Block, et al, Phys. Rev. D41, 978 (1990).
- (2) Amos, et al, Phys. Rev. Letters 26, 2784 (1989); Amos, et al, "A Luminosity-Independent Measurement of the $p\bar{p}$ Total Cross Section at $\sqrt{s} = 1.8$ TeV", accepted for publication in Physics Letters; Amos, et al, "Antiproton-Proton Elastic Scattering at $\sqrt{s} = 1.8$ TeV from $|t| = 0.034$ to 0.65 (GeV/c)²", submitted to Physics Letters.

Part A Figure Captions

Fig. 1 Extrapolations of σ_c , B, and ρ to higher energies based on fits to Fermilab, ISR, and SPS data. See Reference 1. The UA4 ρ -value of $0.24 \pm .04$ has been plotted, but not used in the fit.

Fig. 2 Schematic of an elastic scattering. The measured vertical displacements from the beam are y_1 and y_2 . The measured scattering angle for P_1 is $(y_1')_m = y_1/L_1$ where $L_1 = \sqrt{\beta_x^* \beta_y^*} \sin \psi_1$ is the effective length.

Fig. 3 Plot of dN_{e1}/dt vs. θ for different values of ρ . dN/dt has been normalized to one at $\theta = 10^{-5}$ radians.

Fig. 4 Magnet configuration to achieve $\beta_x^* = \beta_y^* = 2000$ m and $\alpha_x^* = \alpha_y^* = 0$.

Fig. 5 $d\sigma/dt$ vs. τ at $\sqrt{s} = 40$ TeV using the Reference 1 formalism.

Fig. 6 Schematic of scintillating fiber detector. In this view both a top and bottom detector have been pushed in to about 1 mm from the beam.

Fig. 1a

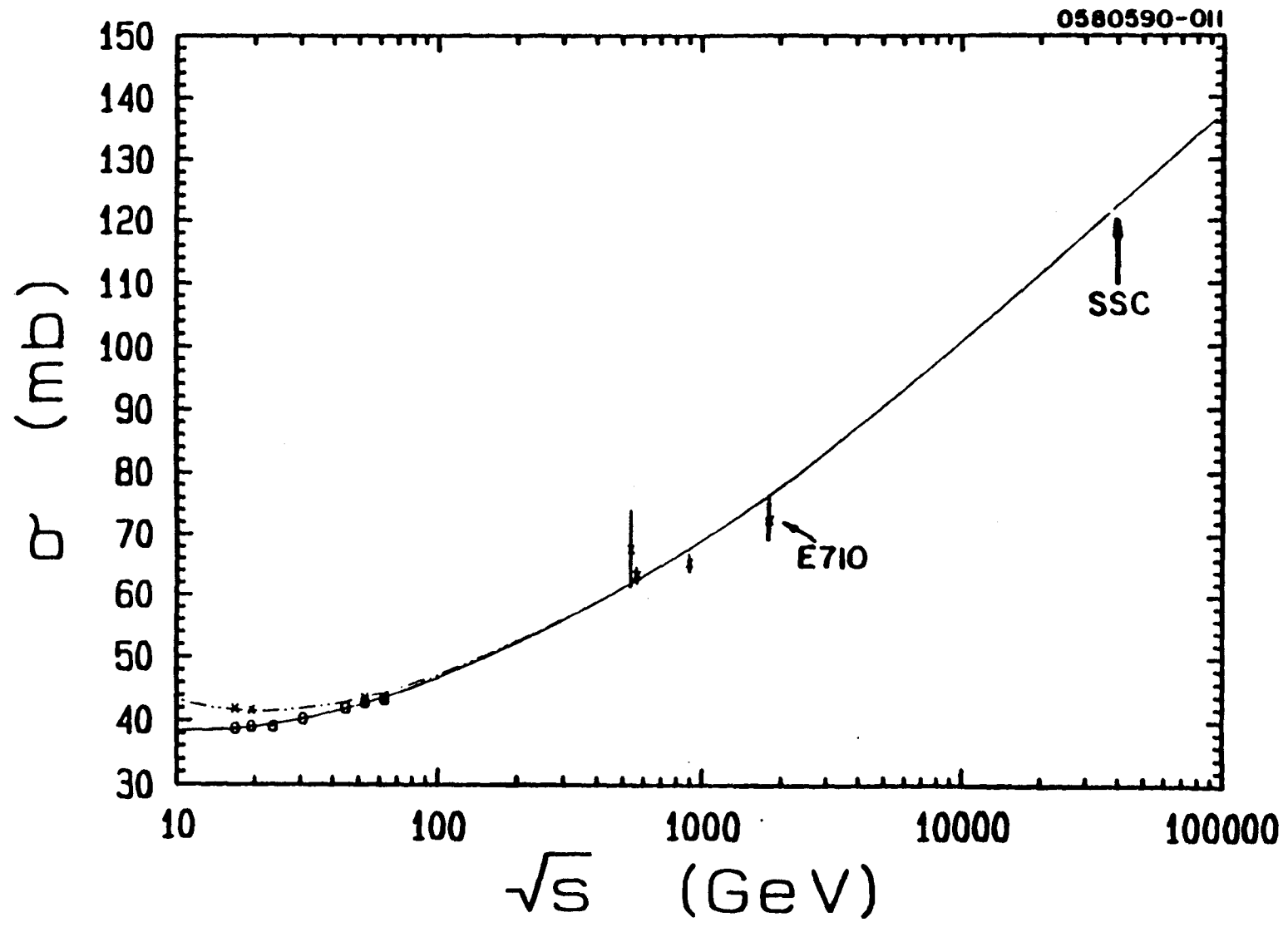


Fig. 1b

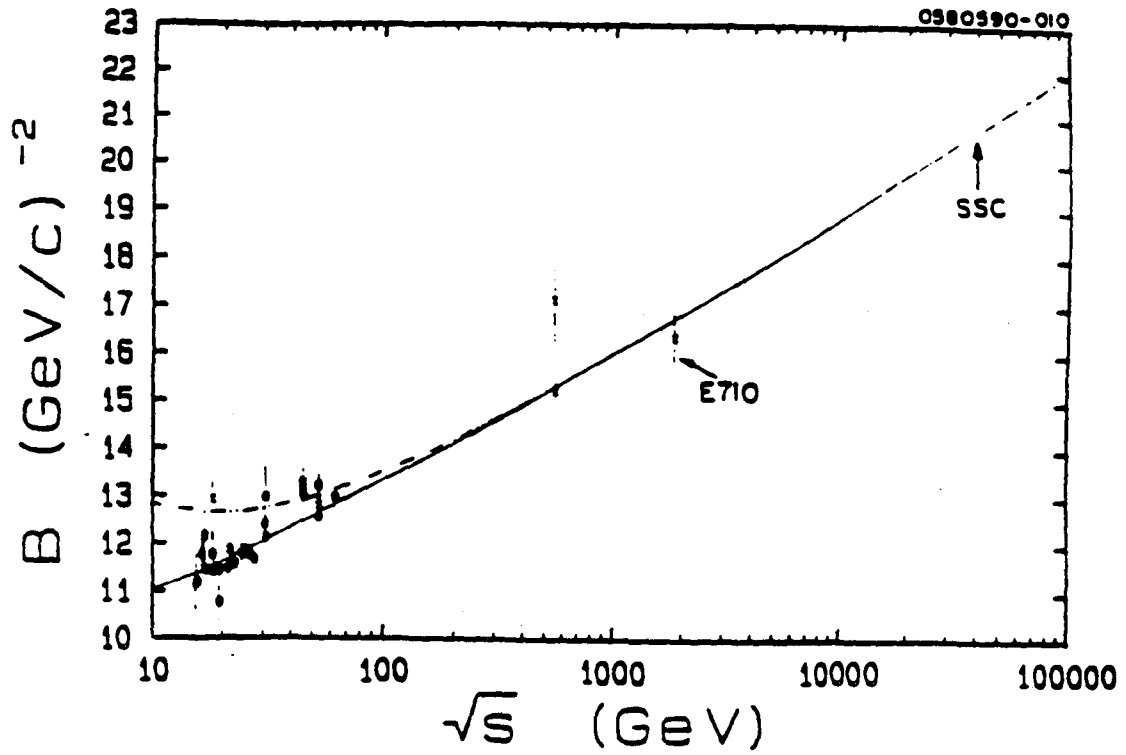
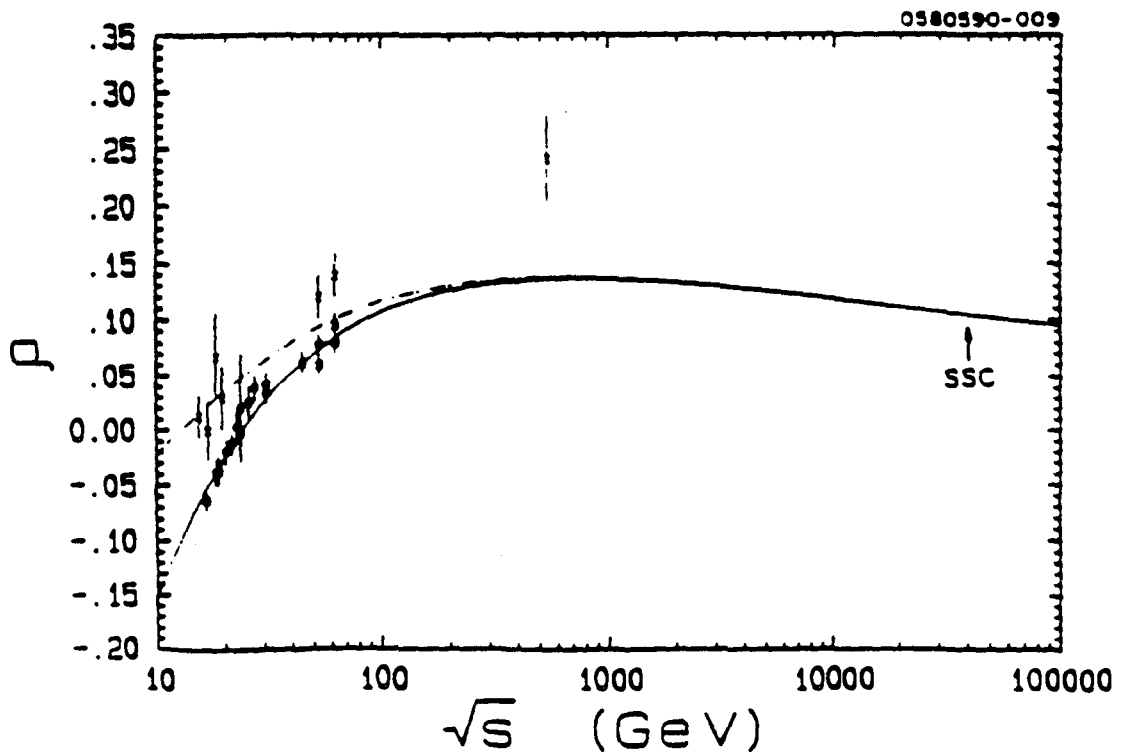


Fig. 1c



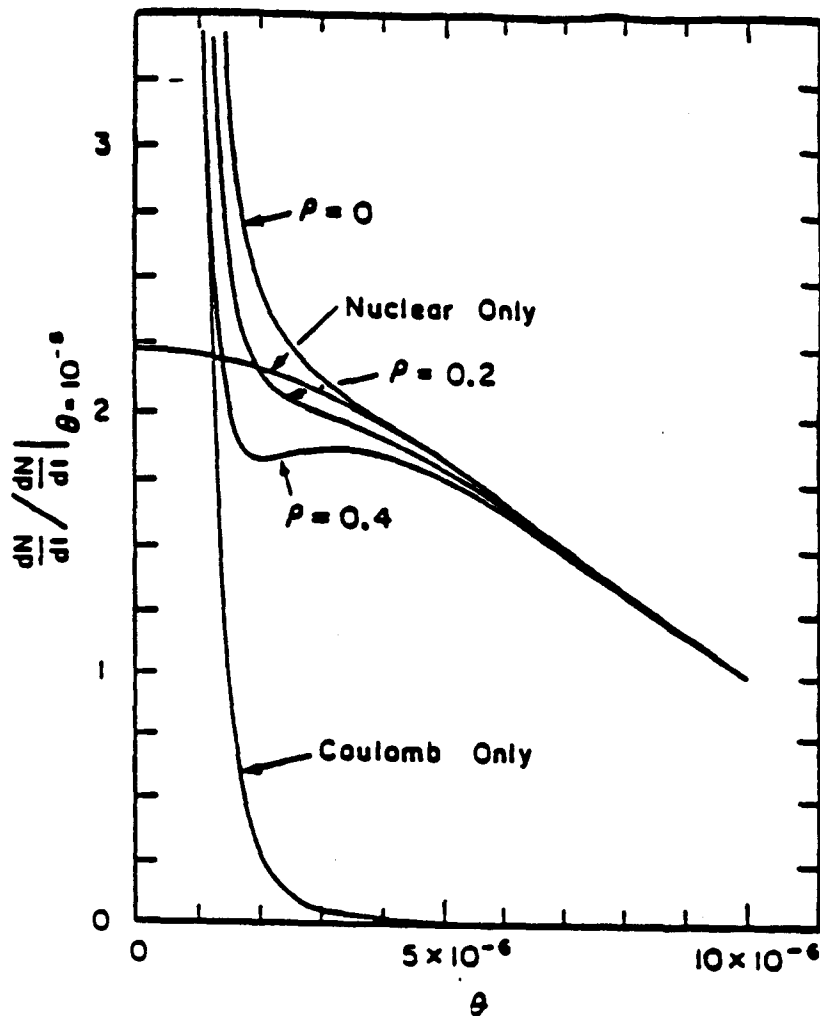


Fig. 3

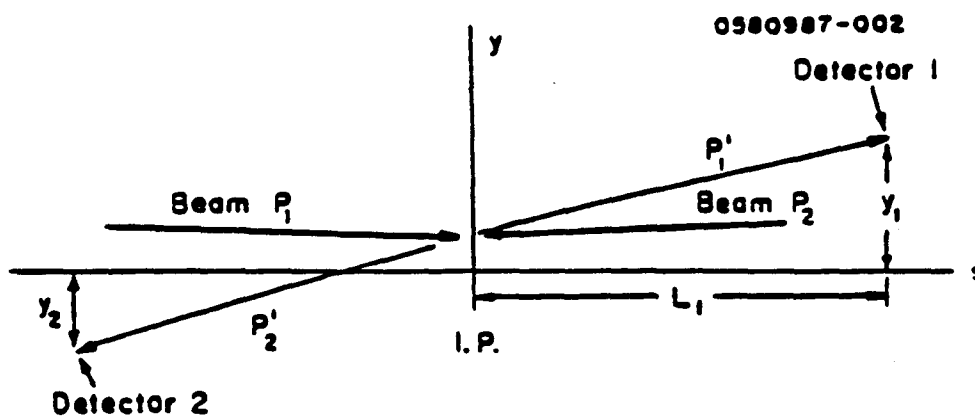


Fig. 2 Schematic of an elastic scattering. The measured vertical displacements from the beam are y_1 and y_2 . The measured scattering angle for P_1 is $(y_1')_m = y_1/L_1$ where $L_1 = \sqrt{(\beta^* \beta_0^*)} \sin \psi_1$ is the effective length.

Fig. 4

$$\beta^m = 2000m, \alpha^m = 20$$

12 April 70

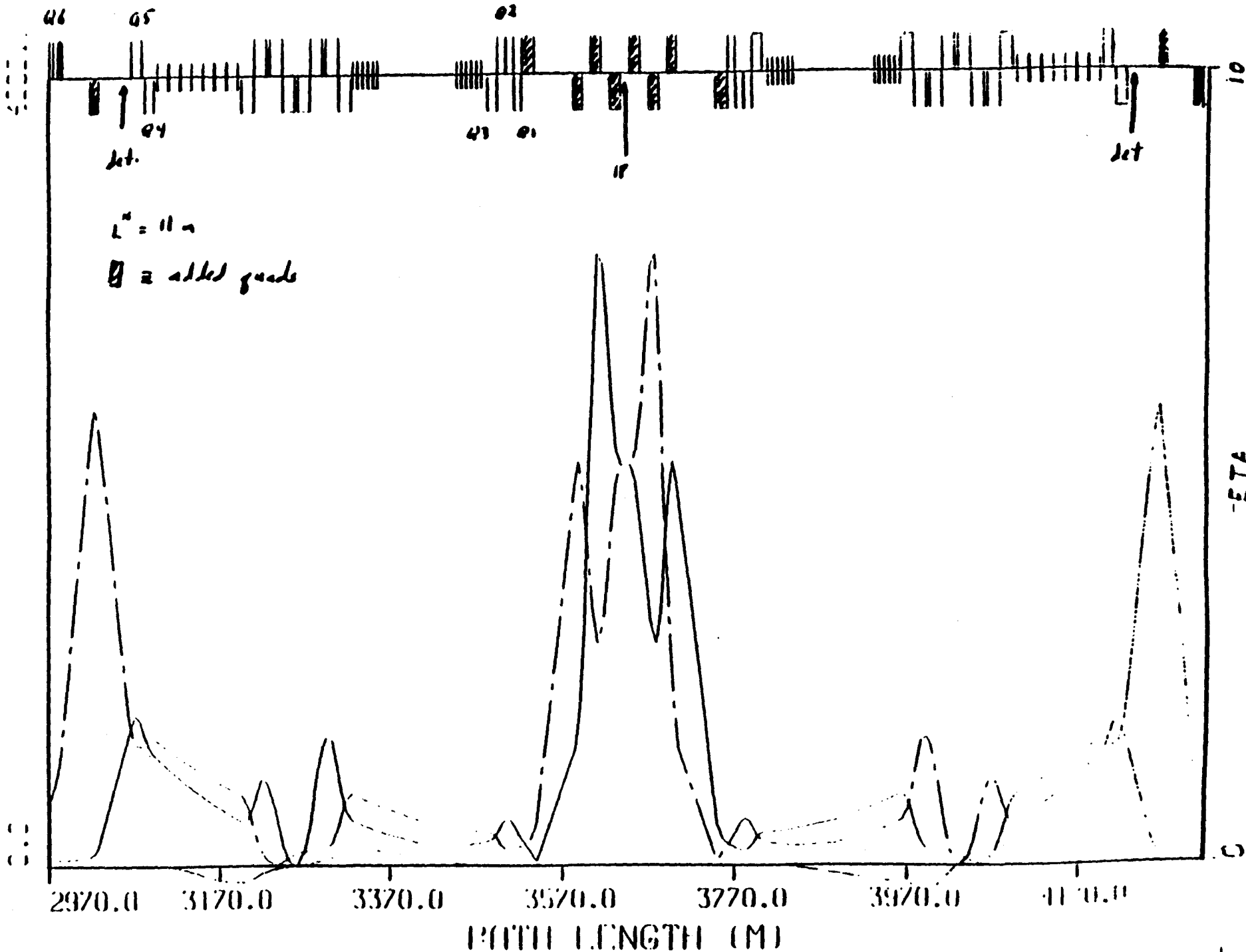


Fig.5

$\sqrt{s} = 40000$ GeV for p-p system

File: 6E05M60.DAT

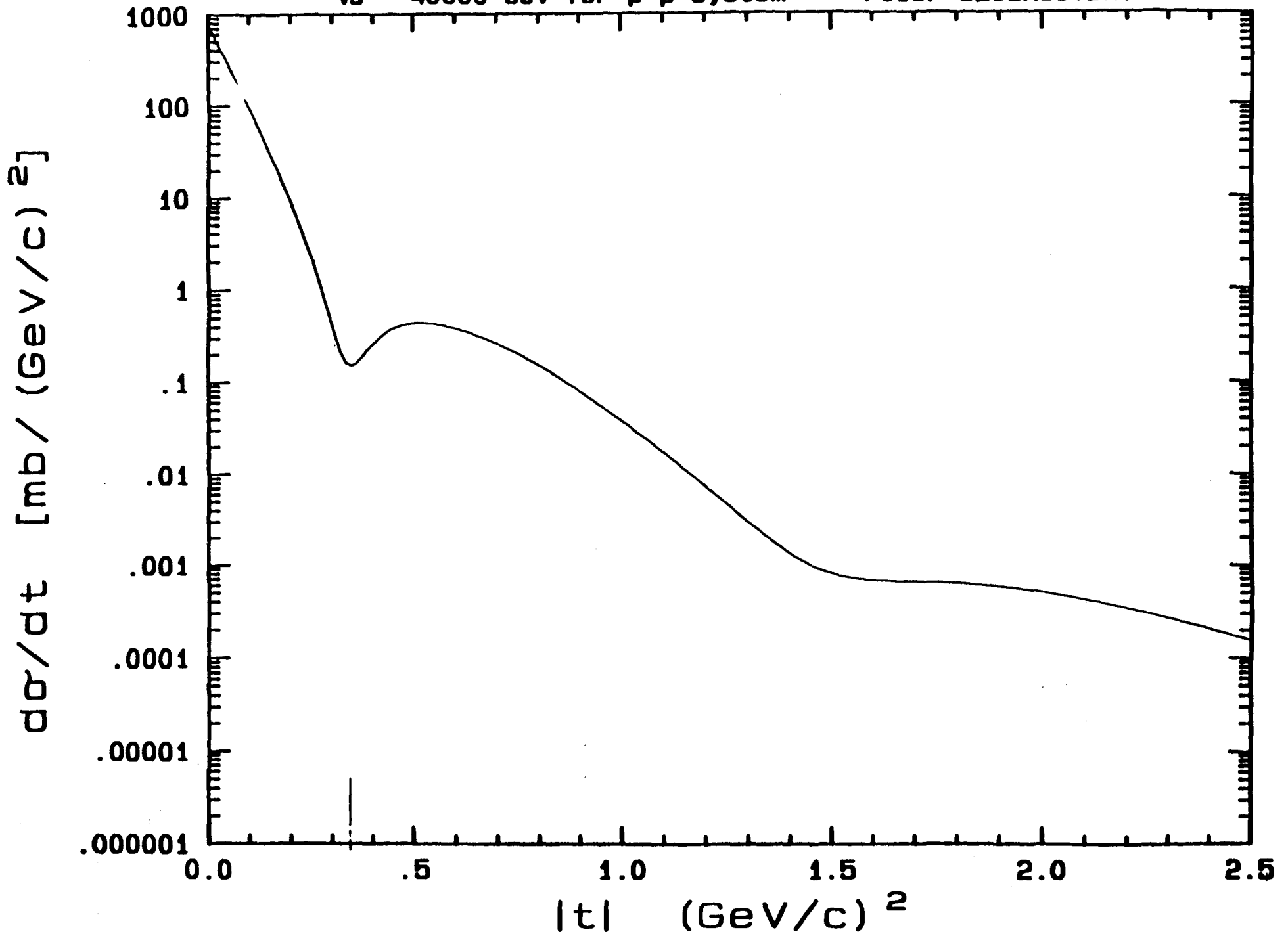
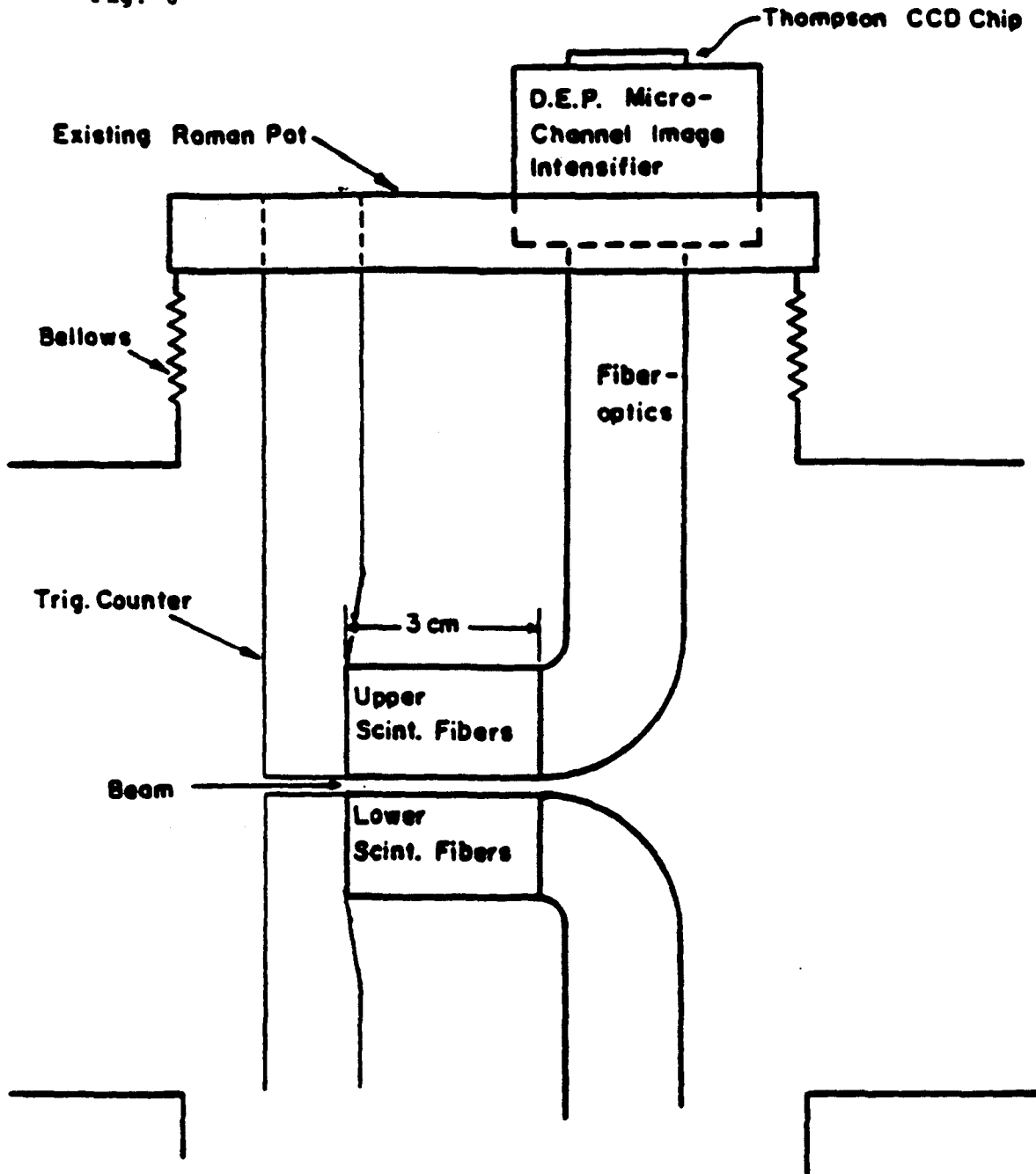


Fig. 6



Modification of Roman Pots for Tevatron

DIFFRACTION DISSOCIATION AT THE SUPERCONDUCTING SUPERCOLLIDER

ABSTRACT

We propose to build "diffractive spectrometers" to measure the momentum of recoil protons from single diffraction dissociation (SD) and double Pomeron exchange (DPE), utilizing the machine magnets and detectors in "Roman Pots". The momentum acceptance will be in the range $4 \times 10^{-4} < 1-x < 0.09$, which corresponds to diffractive masses of 0.8 to 12 TeV and DPE masses of 16 GeV to 3.6 TeV. The spectrometers will be used for measuring differential cross sections and for tagging diffractive masses for further study by general purpose detectors.

1. Introduction.

The study of leading proton diffractive processes, single diffraction dissociation (SD) and double Pomeron exchange (DPE), requires accurate measurements of the angle and momentum of the "recoil" proton(s). These protons, having $\bar{p}_T \sim 270$ MeV and momentum close to that of the beam, are part of the beam halo and therefore they may be conveniently analyzed by spectrometers employing the magnets of the machine itself. We propose to build such "diffractive spectrometers", consisting of detectors in "Roman Pots" stationed in key positions along the main ring on both sides of an interaction point (IP). The Pots will be movable, so that they may be placed near the coasting-beams after injection, making it possible to measure momenta very close to that of the beam. Two types of spectrometers are proposed, designed to cover two regions of "recoil" momentum. Their combined momentum acceptance is in the region $4 \times 10^{-4} < |p - p_{beam}| / p_{beam} < 0.09$, which corresponds to SD masses of 0.8-12 TeV and DPE masses of 16 GeV to 3.6 TeV.

In the sections that follow, we first discuss SD, providing some physics motivation for its study and outlining the kinematics relevant to the design of the spectrometers and the detection of the dissociation products. We then proceed to describe the "diffractive spectrometers", comment briefly on their application to the study of DPE and finish with a discussion of event rates, background and triggering.

2. Single Diffraction Dissociation.

A large fraction of the proton-proton cross section at the SSC is expected to be due to the process of single diffraction dissociation,

$$p + p \rightarrow p + X \tag{1}$$

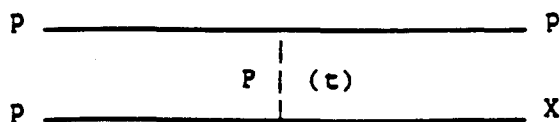


FIG. 1

in which one of the protons is excited coherently into a high mass state X in a low momentum transfer collision. In terms of the Feynman x-variable, $x = 2 p_{11}^* / \sqrt{s}$, the minimum t-value required for excitation into a mass M is given by

$$|t|_{\min}^{1/2} / m_p = 1-x = M^2 / s \quad (2)$$

As $|t|_{\min}^{1/2}$ becomes smaller than the mass of the pion, the "recoil" proton is likely to remain intact, leading to coherent or diffractive-like phenomena. The excited proton state, upon its creation, dissociates immediately into hadrons, hence the name diffraction "dissociation". The "coherence condition" is given by

$$x = \frac{M^2}{s} \leq \frac{m_\pi}{m_p} = 0.15 \quad (3)$$

The differential cross section $d^2\sigma/dt dx$ grows as the process becomes more and more coherent, i.e. as $|t|$ or $1-x$ decrease. The growth at small $|t|$ follows the well known exponential behavior of classical diffraction, which is also observed in elastic scattering. The increase of the cross section at small $1-x$ is a purely quantum-mechanical phenomenon involving momentum transfer in the forward rather than in the transverse direction, which kinematically must be associated with a change in mass. Fig. 2 shows the cross section versus $1-x$ for $pp \rightarrow pX$ at $s = 500 \text{ (GeV)}^2$. The enormous peak in the region $1-x \leq 0.15$ is attributed to diffraction dissociation [1].

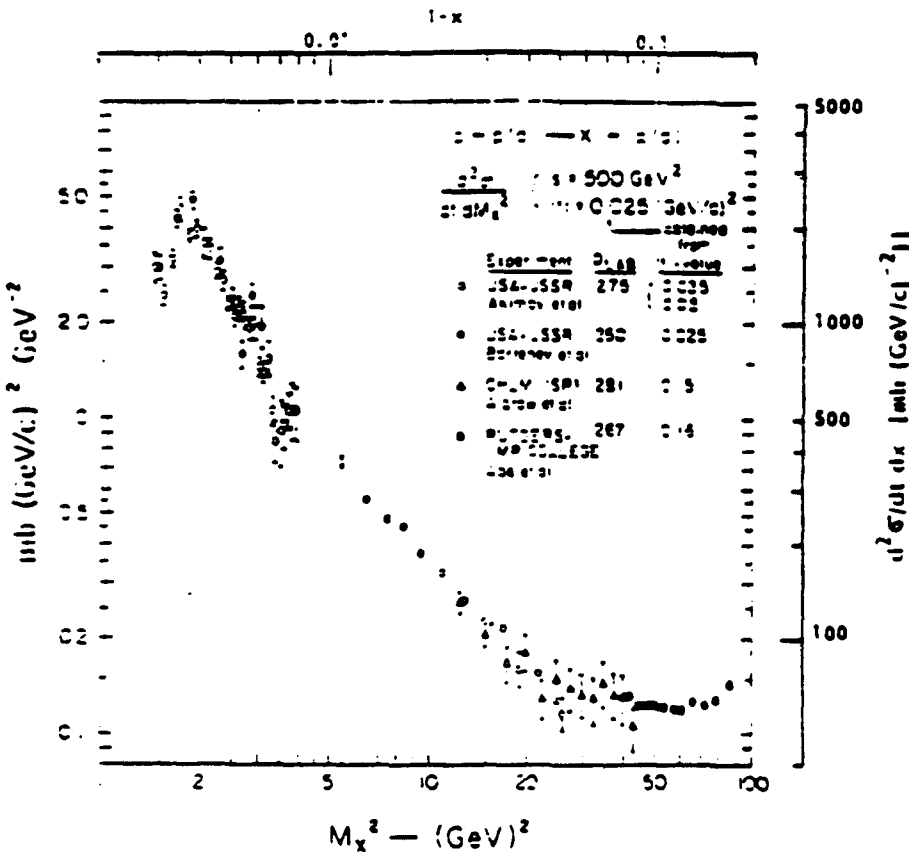


FIG.2: The differential cross section $d^2\sigma/dt dx$ versus M^2 for $pp \rightarrow pX$ at $t = -0.025 \text{ (GeV/c)}^2$ and $s = 500 \text{ GeV}^2$. The axes on top and right give $d^2\sigma/dt dx$ versus $1-x$.

Within the diffractive peak, the cross section $d^2\sigma/dt dM^2$ varies as $1/M^2$ and obeys factorization and the finite mass sum rule. This behavior is consistent with the hypothesis that diffraction dissociation is dominated by Pomeron exchange. In the mass region $5 \text{ GeV}^2 < M^2 < 0.15s$ and for $|\tau| < 0.1$ $(\text{GeV}/c)^2$, a useful parametrization of the diffractive cross section is given by [1]:

$$\frac{d^2\sigma}{dt dM^2} = \frac{A}{M^2} (b e^{b\tau}) \quad (4)$$

where $A = 0.7 \pm 0.05 \text{ mb}$ and $b / b_{e_2} = 1/2$ to $2/3$. At the SSC, the elastic slope is expected to be [2] around $24 (\text{GeV}/c)^2$ and therefore $b = 14 (\text{GeV}/c)^2$. The average $|\tau|$ of the diffractive states is thus $|\tau|_{\text{ave}} = 1/b = 0.07 (\text{GeV}/c)^2$, corresponding to an average production angle of $-13 \mu\text{rad}$. The total single diffraction dissociation cross section, obtained by integrating Eq. 4 over τ and M^2 from threshold ($\approx 1 \text{ GeV}^2$) to $0.15s$, is given by $\sigma_{SD} = 2 A \ln(0.15s / \text{GeV}^2)$, where the factor of 2 accounts for the fact that both protons may dissociate. At $\sqrt{s} = 40 \text{ TeV}$, $\sigma_{SD} = 27 \text{ mb}$, which is roughly 20 % of the expected [2] total cross section of $\approx 120 \text{ mb}$.

The Pomeron plays an important role not only in SD but also in all other diffractive processes, such as elastic scattering, double diffraction dissociation (DD), IFF and in the total cross section, which is related to elastic scattering through the optical theorem. The QCD description of these "soft" processes will invariably involve a Pomeron-like theoretical structure. In order to formulate such a structure, one needs to know the cross sections of the above processes, commonly referred to as "lns physics", and the nature and properties of the dissociation products, the physics known as "hard diffraction". There is an abundance of theoretical models predicting large heavy flavor or gluon-jet content in hard diffraction, although the theoretical community is not unanimous in its opinion. In view of the small momentum transfer in diffractive processes, it has even been conjectured [3] that the "Pomeron energy" transferred in high mass SD may heat the proton receiving it to very high temperatures, leading to a QCD phase transition at relatively low diffractive masses ($\approx 100 \text{ GeV}$), a process that might explain the Centauro-type events observed in cosmic rays. Be as it may, the study of hard diffraction is certainly interesting!

At the SSC, masses as high as 15 TeV fall within the region of the coherence condition, Eq. 3. Although, as pointed out above, the production angles of the masses themselves are small, the angles of their dissociation products are generally quite large. The kinematics of SD are summarized in Figs 3, 4 & 5.

Fig. 3 shows the expected shape of the pseudorapidity distribution of a diffractive cluster of mass M . The average η is $\bar{\eta}_M = \ln(\sqrt{s}/M)$. The average laboratory angle, obtained by using the relation $\eta = -\ln \tan(\theta/2)$, is given by

$$\bar{\theta}_M = 2 M/\sqrt{s} = 2 \sqrt{1-x} \quad (5)$$

Thus, masses in the range 0.8-12 TeV, tagged by the proposed spectrometers, dissociate into clusters of average angle 40-600 mrad. Such large angles are easily covered by general purpose detectors that have been proposed for the SSC.

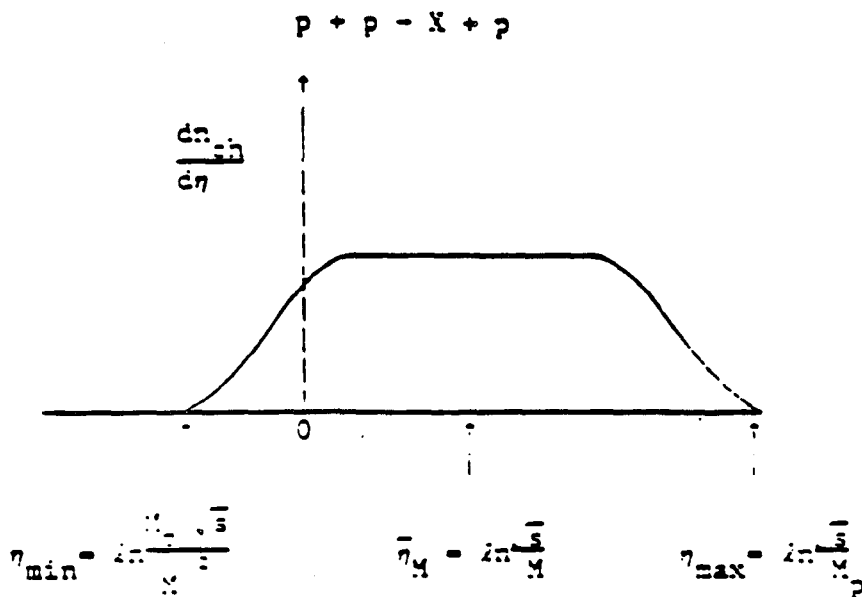


FIG. 3. Schematic drawing of the charged particle pseudorapidity distribution of a diffractive cluster of mass M created in a $pp\text{-}Xp$ collision at \sqrt{s} .

Fig. 4 shows the cross section $d\sigma/d\bar{\eta}_M$ as a function of $\bar{\eta}_M$. From Eq. 4 and $\bar{\eta}_M = \ln(\sqrt{s}/M)$, it follows that $d\sigma/d\bar{\eta}_M = 2A$, i.e. the cross section is flat and has the value $2A = 1.4$ mb. The shaded area in the figure represents the region that can be tagged by the diffractive spectrometers. Clusters from beam-gas non-diffractive collisions will be centered at $\bar{\eta} = \eta_{\max}/2 = 5.3$. However, particles from such collisions will spread over the entire hemisphere, from $\eta = 0$ to $\eta = 10.6$.

Fig. 5 shows the η -distributions expected for diffractive clusters of different masses (see also Fig. 3). The beam-gas clusters are also shown. Beam-gas events will be vetoed in the trigger stage by requiring coincidence between the recoil proton and the diffractive cluster.

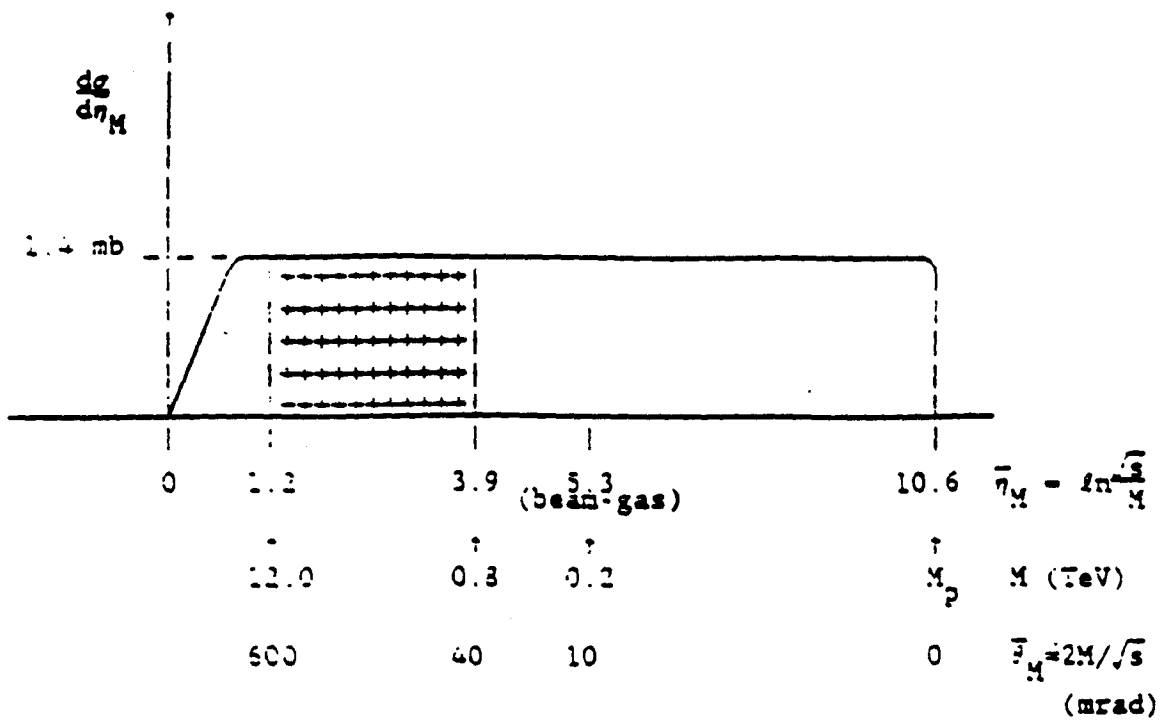


FIG. 4: Single diffraction dissociation cross section $dg/d\bar{\eta}_M$ versus $\bar{\eta}_M$, where $\bar{\eta}_M$ is the average pseudorapidity of a cluster of mass M . The crossed area corresponds to the acceptance of the "diffractive spectrometers".

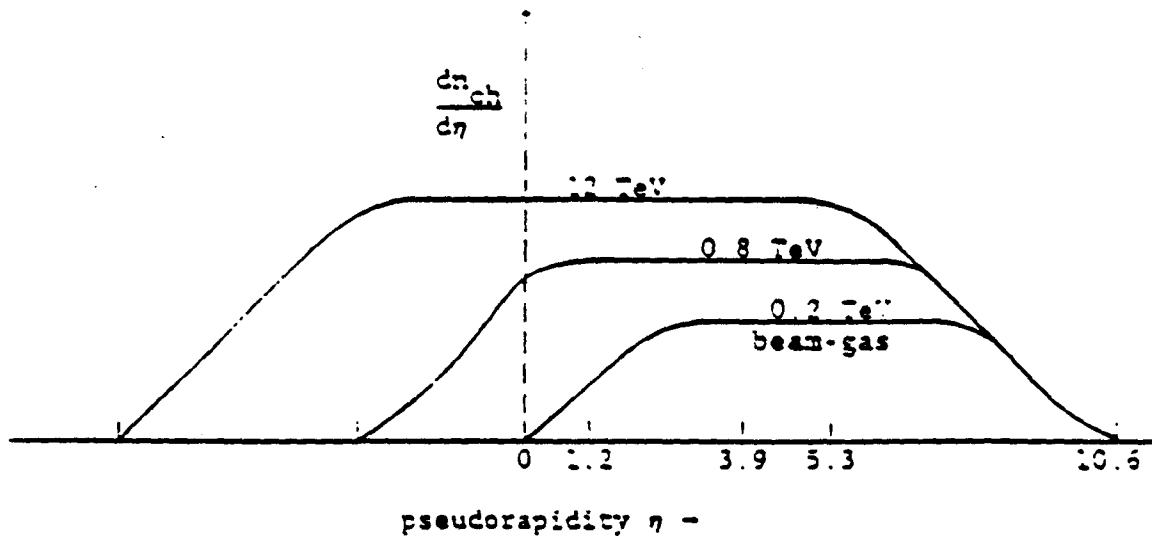


FIG. 5: Charged particle pseudorapidity distribution for various mass values.

3. The "Diffractive Spectrometers".

The diffractive spectrometers consist of detectors in "Roman Pots" located at appropriate stations along the main ring on both sides of an IP. The position of the Pots is controlled remotely, so that they may be kept away from the beam during injection and moved close to it after stable coasting conditions are attained. Particles created at the IP within a certain angular and momentum range are detected and their momentum is magnetically analyzed using the magnets of the machine itself. The fractional difference of the particle's momentum from the momentum of the beam is related to the diffractive mass (see Eq. 3):

$$\frac{\Delta p}{p} = 1-x = \frac{M^2}{s} \quad (6)$$

The diffraction region spans approximately the range $(2 \text{ GeV}^2/s) < 1-x < 0.15$ with the lower value corresponding to excitation of the proton to isobars. If the cross section continues to grow as $1/(1-x)$ at the SSC, the diffractive peak of Fig. 2 is expected to reach a height of eight orders of magnitude! The diffractive spectrometers should be designed to cover as much of this range as possible. However, as we shall see, there are limitations that restrict the accessible region to $4 \times 10^{-4} < 1-x < 0.09$, corresponding to diffractive masses of 0.8-12 TeV. Fortunately, the mass region below 0.8 TeV can be covered by the Fermilab Tevatron ($\sqrt{s} = 2 \text{ TeV}$).

We have designed two types of spectrometers, a horizontal and a vertical one, covering two different regions of $1-x$. Below, we discuss the design characteristics of each type.

(a) The horizontal spectrometers.

A particle created at 0° with momentum close to but smaller than that of the beam settles into an orbit of smaller average radius. Particles of the same momentum but at small angles with respect to the beam exhibit betatron oscillations around their mean orbit. The horizontal spectrometers consist of a system of instrumented Pots placed at appropriate positions to detect particles that have been captured within the aperture of the machine and circulate as beam halo. The displacement of such particles from the beam axis is determined by the "lattice functions" $\beta_{x,y}$ and $\eta_{x,y}$. Fig. 6 shows values of the lattice functions in the vicinity of a medium beta interaction region (IR). The loss of momentum leads to a horizontal displacement $\Delta x = \eta_x (\Delta p/p)$ and the change in angle results in oscillations

of amplitude $\Delta \theta x L_{\text{eff}}$, where $L_{\text{eff}} = (\beta_x \beta_x^*)^{1/2}$. Fig. 7 shows the path of particles in a region far enough from the IP, where normal periodic conditions are re-established. Detectors placed at the indicated locations comprise the spectrometer. Two of the locations are also shown in Fig. 6. The detectors on the outer side of the beam are used for measuring elastic scattering in conjunction with the mirror image of this arrangement on the other side of the IP, which is also necessary for the study of DPE.

The acceptance of the spectrometer is limited on the high momentum side by the size of the beam, which determines the minimum approach of the detectors to the beam axis (-10σ is considered "safe") and on the low side

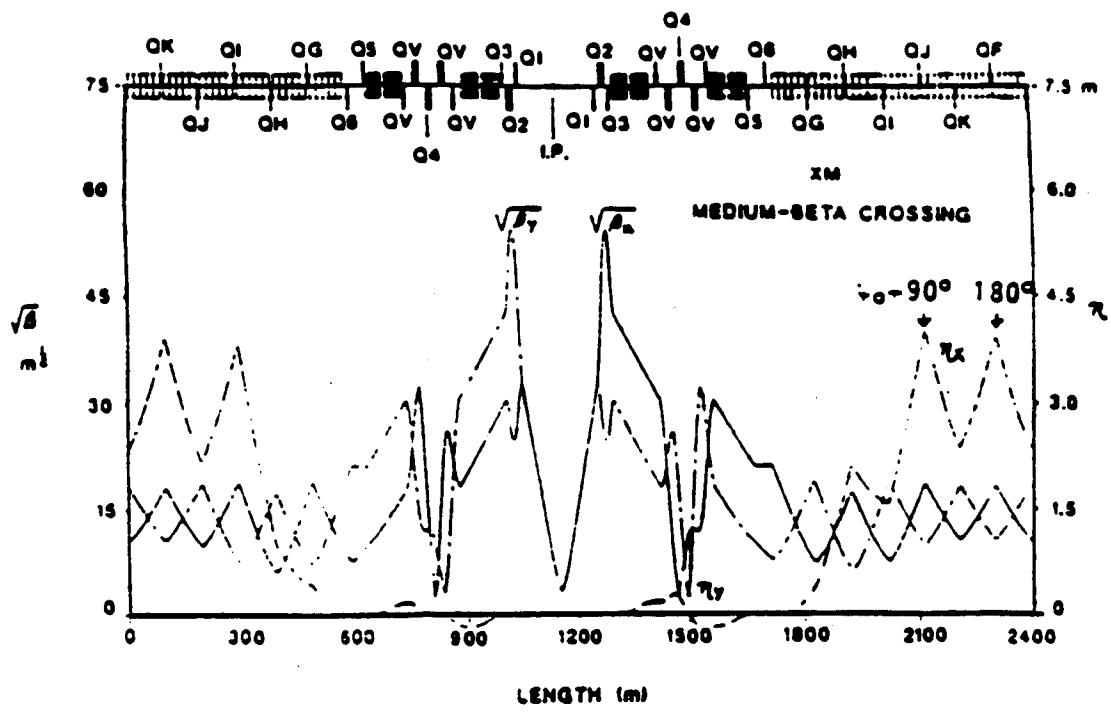


FIG. 6: Lattice functions in the vicinity of a medium-beta crossing IR.

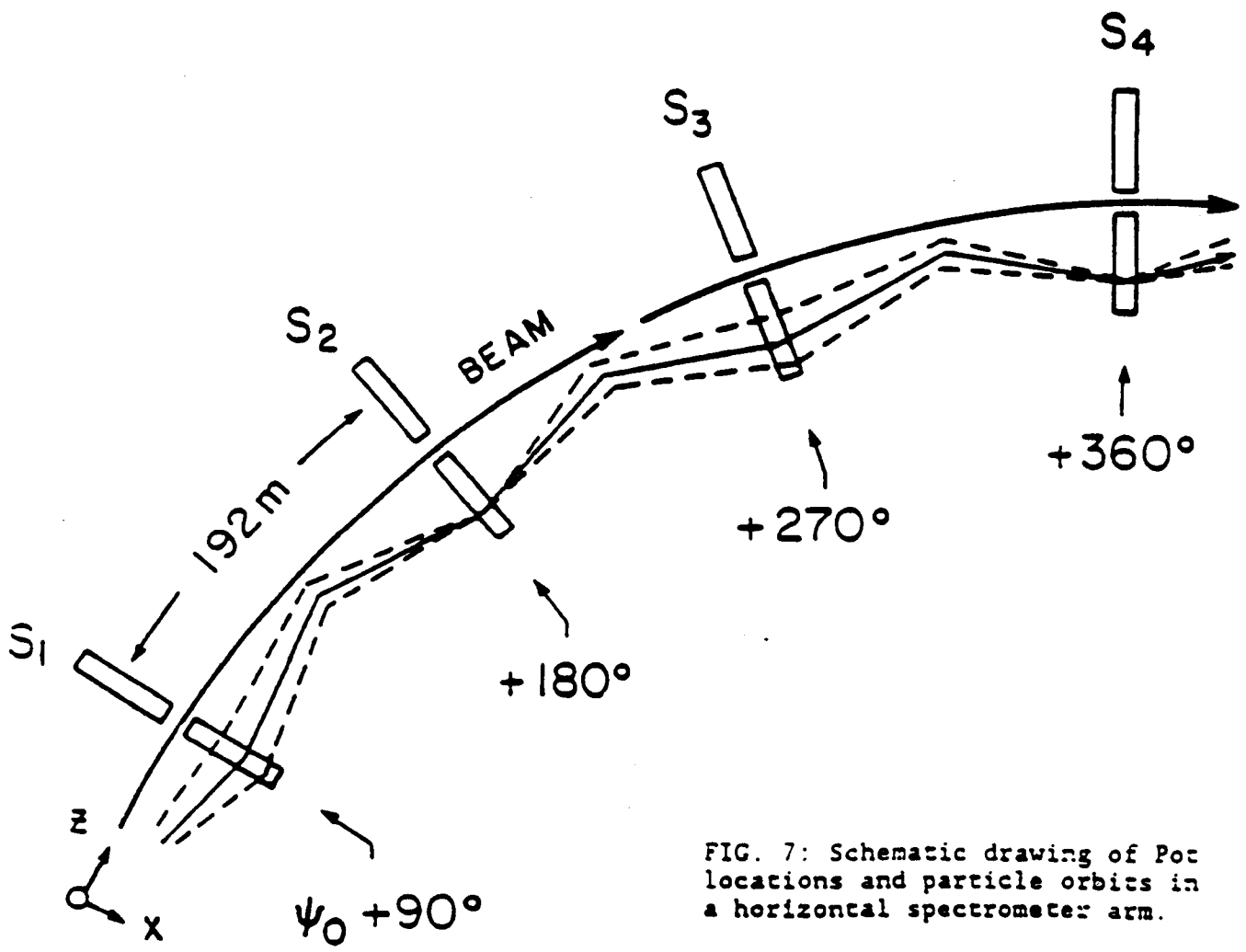


FIG. 7: Schematic drawing of PoC locations and particle orbits in a horizontal spectrometer arm.

by the size of the beam pipe, which has a diameter of 32 mm. The following equations are useful in evaluating the parameters of the spectrometer:

$$\Delta x = \eta_x \frac{\Delta p}{p} \quad (7a)$$

$$L_{\text{eff}} = (\beta_x \beta_x^*)^{1/2} \quad (7b)$$

$$\sigma_x = (\epsilon \beta_x / \gamma)^{1/2} \quad (7c)$$

$$|\epsilon|_{\text{el}} = [(\Delta x_{\text{at } 90^\circ} / L_{\text{eff}}) p_{\text{beam}}]^{1/2} \quad (7d)$$

Table I shows some characteristics of the horizontal spectrometer, which have been calculated using the values $\eta_x = 2.5$ m, $\beta_x = 250$ m, $\beta_x^* = 10$ m and normalized emittance $\epsilon = 10^{-6}$ m-rad. The beam width at the location of the Pots turns out to be $\sigma_x = 110 \mu$, so that a 1 mm minimum distance of the detectors from the beam should be attainable. As already mentioned, the maximum distance of 15 mm is imposed by the beam pipe.

Table I. Characteristics of the Horizontal Spectrometers.

Distance from beam mm	$\Delta p/p$ (1-x)	Mass M (for $\tau=0$) TeV	Mass Resolution dM/M	Elastic $ \epsilon $ (GeV/c) ²
1	4×10^{-4}	0.8	8.3 %	0.16
2.5	1×10^{-3}	1.3	3.3 %	1.0
15	6×10^{-3}	3.1	0.6	36

The mass resolution is calculated from the momentum resolution using Eq. 6, which yields

$$\frac{dM}{M} = \frac{d(\Delta p/p)}{M^2/s} = \frac{d(\Delta p/p)}{1-x} \quad (8)$$

The momentum resolution has two contributions: One from the dispersion in the beam itself,

$$(\Delta p/p)_{\text{beam}} = 5 \times 10^{-5} \quad (9)$$

and the other from the uncertainty in the measurement of Δx , which is dominated by the beam width of 110μ (we assume that the detector spatial resolution is $\sim 25 \mu$). Using Eq. 7a, we then obtain

$$d(\Delta p/p)_{\text{position}} = \sigma_x / \eta_x \quad (10)$$

Combining (9) and (10) in quadrature results in a total $d(\Delta p/p) = 6.7 \times 10^{-3}$ which substituted into (8) gives the values listed in Table I.

The determination of the absolute value of the mass requires knowledge of the absolute position of the Pots relative to the beam. This is obtained by employing two Pots at every station, one on each side of the beam, whose separation is known. Placing the Pots at equal distance from the beam, which can be done by demanding symmetry in the observed elastic scattering events, gives the distance of each one from the beam as one half of their separation.

A final point to be made is that there are four detector stations in each spectrometer arm, as shown in Fig. 7. At two of the stations, those at phase angles $\psi_0 + 180^\circ$ and $\psi_0 + 360^\circ$, particles of the same momentum (same mass) but created at different angles (different τ -values) register at the same x-position. These detectors may therefore be thought of as "diffractive mass spectrometers". The other two detectors are useful in determining the τ -value. The system of four detectors provides the necessary redundancy.

(b) The Vertical Spectrometers.

Protons created with momentum such that $\Delta p/p > 6 \times 10^{-3}$ do not register in the horizontal spectrometers. In order to extend the acceptance to larger values of $\Delta p/p$ (hence larger masses), we propose the "vertical spectrometers", which take advantage of the vertical crossing magnet arrangement at the IP (Fig. 8). A schematic drawing of the Pot locations is shown in Fig. 9. In Table II we list the spectrometer characteristics, obtained from Eq. 7 with y substituted for x , using the values $\eta_y = 0.175$ m,

$S_y = 200$ m and $\beta^* = 10$ m, which are appropriate for these locations. The beam width is calculated to be $\sigma_y = 100 \mu$. The mass resolution is obtained from Eq. 8, with $d(\Delta p/p)$ dominated now by the position resolution, which has the value $-\sigma_y / \eta_y = 5.7 \times 10^{-4}$.

Table II. Characteristics of the Vertical Spectrometers.

Distance from beam mm	$\Delta p/p$ (1-x)	Mass M (for $\tau=0$) TeV	Mass Resolution dM/M	Elastic $ t $ (GeV/c) ²
1	5.7×10^{-3}	3.0	5 %	0.2
2.25	1.3×10^{-2}	4.5	2.5 %	1
5	2.9×10^{-2}	6.8	1.1 %	5
15	0.09	12	0.4	58

As with the horizontal spectrometers, two Pots are used at each location, one approaching the beam from the top and the other from the

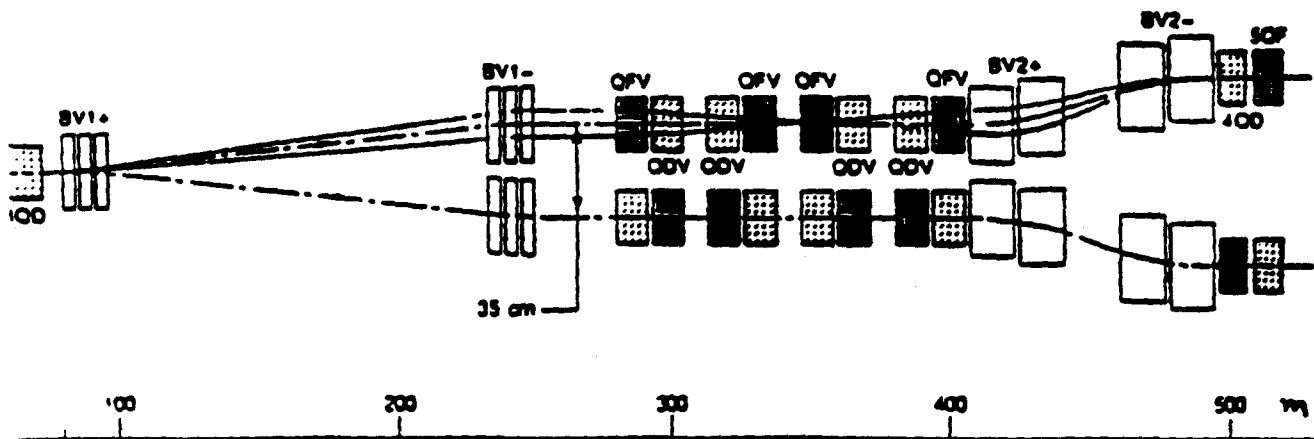


Fig. 8: Magnet arrangement at a low-beta IR vertical crossing (90° lattice). The arrangement at the medium-beta IR's is similar.

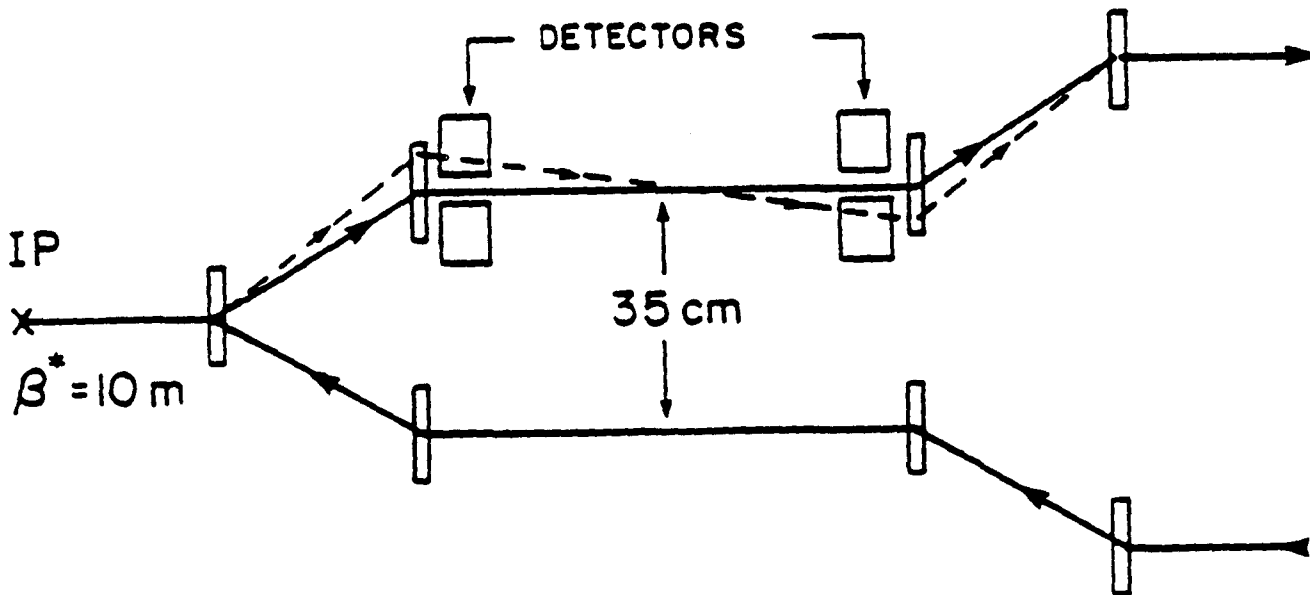


FIG. 9: Schematic drawing of Pot location in a vertical spectrometer arm. The broken line represents the path of a $c = 0$ "leading proton" created at the IP.

bottom. Elastic events will be used again to position the Pots symmetrically with respect to the beam. The employment of two stations in each arm of the spectrometer is necessary for the simultaneous determination of the momentum and τ -value. A mirror image arrangement on the other side of the IP is required for the study of elastic scattering and double Pomeron exchange.

4. Double Pomeron Exchange (DPE).

Double Pomeron exchange is characterized by two leading protons, each having the properties (τ and x distribution) of the recoil proton in single diffraction dissociation:

$$p + p \rightarrow p + p + X \quad (11)$$

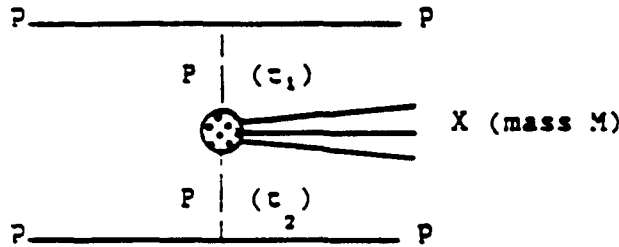


FIG. 10

The proposed diffractive spectrometers may therefore be used to study this process, provided they are installed on both sides of an IP. As already mentioned, such an arrangement is also necessary for the study of elastic scattering.

The main interest in DPE is in probing the structure of the Pomeron in pure Pomeron-Pomeron collisions. The differential cross section is also of interest as it provides a strict test of factorization.

The kinematics and cross sections of DPE are summarized below:

$$\frac{M^2}{s} = (1-x_1)(1-x_2) \quad y_M = \frac{1}{2} \ln \frac{1-x_1}{1-x_2} \quad (\text{rapidity of mass } M)$$

$$\frac{d^4 \sigma}{d\tau_1 dx_1 d\tau_2 dx_2} = \frac{1}{\sigma_T} \frac{d^2 \sigma_1}{d\tau_1 dx_1} \frac{d^2 \sigma_2}{d\tau_2 dx_2}$$

$$\text{where } \frac{d^2 \sigma}{d\tau dx} = \frac{A}{1-x} (b e^{d\tau}) \quad ; A = 0.7 \text{ mb}$$

$$\frac{d^2 \sigma}{d(M^2/s) dy} = \frac{1}{\sigma_T} \frac{M^2}{s} \quad \frac{d\sigma}{dM^2} = \frac{1}{\sigma_T} \frac{A^2}{M} \ln^2 (M_{\text{max}} / M)^2$$

$$\sigma = 2 \frac{A^2}{\sigma_T} \ln^2 \frac{M_{\text{max}}}{M_{\text{min}}}$$

The momentum acceptance of our diffractive spectrometers, $4 \times 10^{-4} < 1-x < 0.09$, corresponds to DPE masses in the range

$$16 \text{ GeV} < M < 3.6 \text{ TeV}$$

The accepted cross section is 0.24 mb, which is about 40 % of the total DPE cross section. The mass resolution varies from -12 % at low masses to -0.6 % at 3.6 TeV. Clearly, the proposed double arm diffractive spectrometers are very well suited to study the very promising DPE process.

5. Event rates, background and triggering.

Studies of "hard diffraction" require high luminosity. However, since events must be tagged, such studies cannot be performed in a high beta IR ($\beta^* = 0.5$), where the average number of interactions per bunch crossing is expected to be ~ 1.5 . The medium beta IR's, with $\beta^* = 10 \text{ m}$ and a design luminosity of $5.6 \times 10^{31} / \text{cm}^2$, are better suited for diffractive tagging. The SD cross section within the mass acceptance of each spectrometer (horizontal or vertical) is $\sim 1.9 \text{ mb}$, which is reduced to $\sim 1 \text{ mb}$ by the x -acceptance. The expected SD "recoil" proton rate in each spectrometer arm is then $\sim 6 \times 10^4 / \text{sec}$.

The detectors will, of course, also be counting particles from beam-gas interactions. As an estimate of beam-gas rates, we note that at a pressure of 10^{-9} Torr of hydrogen, the number of interactions expected to occur in a 100 m pipe length is $\sim 10^4 / \text{sec}$. Such rates are relatively small and can be handled by requiring coincidence between the spectrometers and the diffractive clusters.

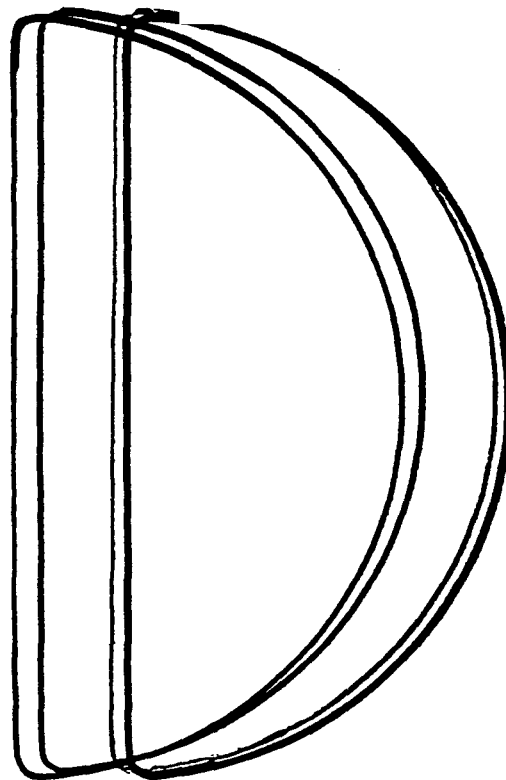
A more serious problem is posed by the beam halo created at the low beta, high luminosity IR's. As much as 10 % of the pp cross section results in leading protons being captured in the machine, creating a halo at a rate of $\sim 10^7 / \text{sec}$. It is imperative that these protons be removed by the use of beam scrapers. Assuming that the halo is "killed" within a few revolutions, the equilibrium rate is expected to be $\sim 10^4 / \text{sec}$, which is again tolerable.

References.

1. K. Goulianos, Physics Reports Vol.101, No.3, December 1983.
2. K. Goulianos, "Diffractive and Rising Cross Sections", Proceedings of Workshop on Physics Simulations at High Energy, University of Wisconsin-Madison, 5-16 May 1986, World Scientific (Edited by V. Barger, T. Gottschalk and F. Halzen) pp. 127-140. Also: To be published in "Comments on Nuclear and Particle Physics, Gordon and Breach, Science Publishers, Inc.
3. K. Goulianos, "A Model for Centauro Production", Proceedings of Workshop on Physics Simulations at High Energy, University of Wisconsin-Madison, 5-16 May 1986, World Scientific (Edited by V. Barger, T. Gottschalk and F. Halzen) pp. 299-312. Also: To be published in "Comments on Nuclear and Particle Physics, Gordon and Breach, Science Publishers, Inc.

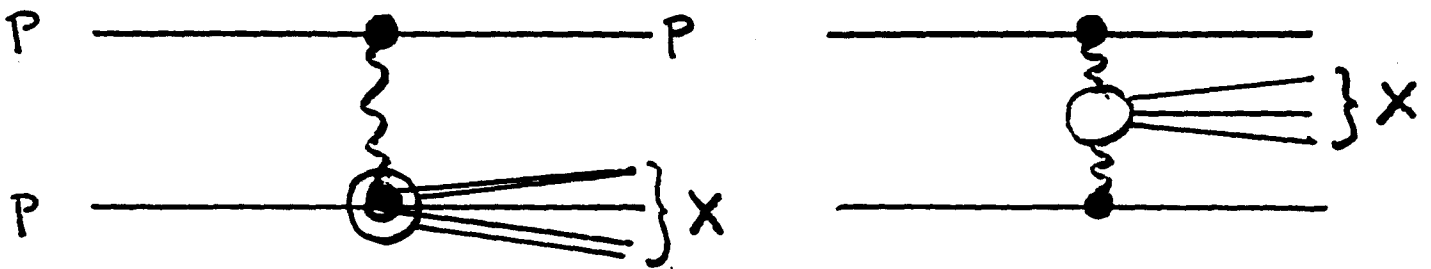


DIFFRACTION AT THE SSC
An Expression of Interest
June 7-9, 1990



Dino Goulianos
Rockefeller University

Tagging High Mass Diffraction at the SSC



$$q_{\parallel} \lesssim m_{\pi} \Rightarrow \text{COHERENCE}$$

$$\frac{|q_{\parallel}|}{m_p} \approx \frac{M_x^2}{s} = 1-x \lesssim 0.1$$

SINGLE
DIFF.

$$M_x \lesssim \sqrt{0.1s} \approx 12 \text{ TeV}$$

DOUBLE
POMERON

$$M_x \lesssim 0.1\sqrt{s} \approx 4 \text{ TeV}$$

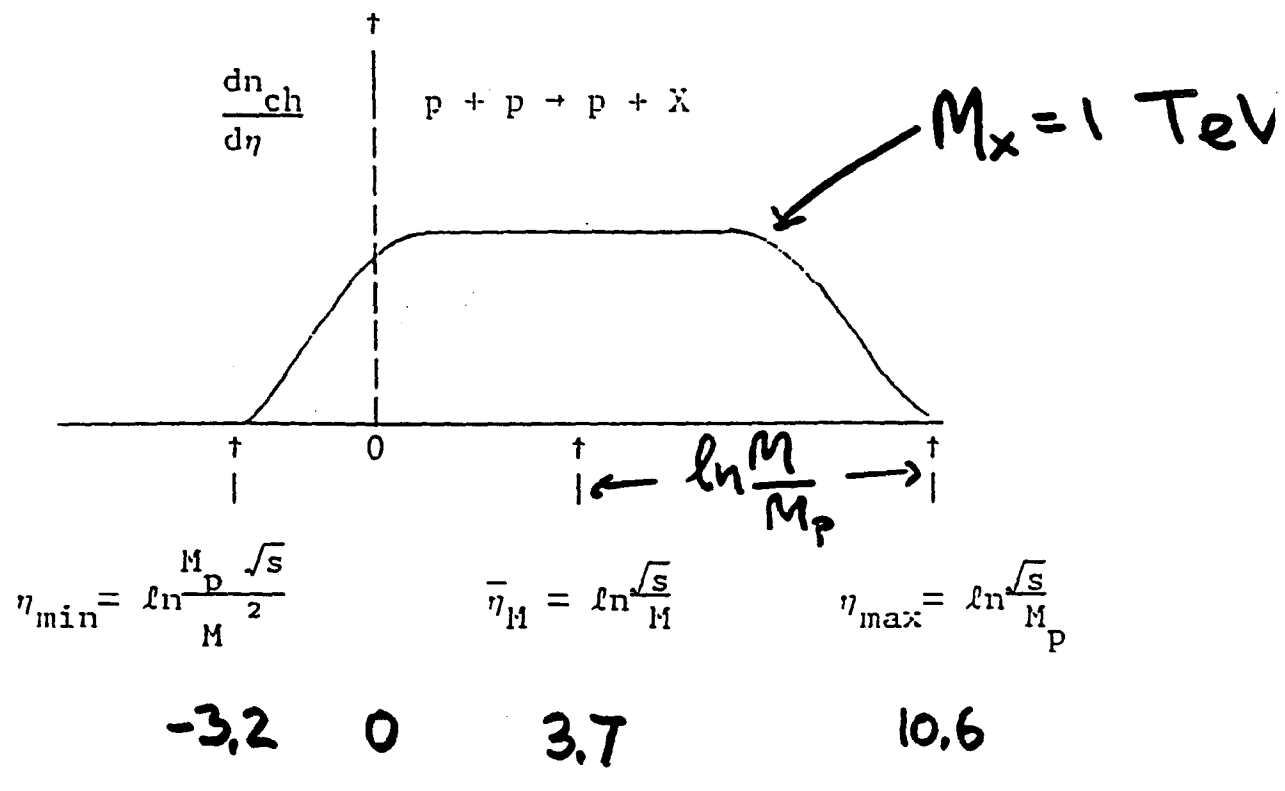
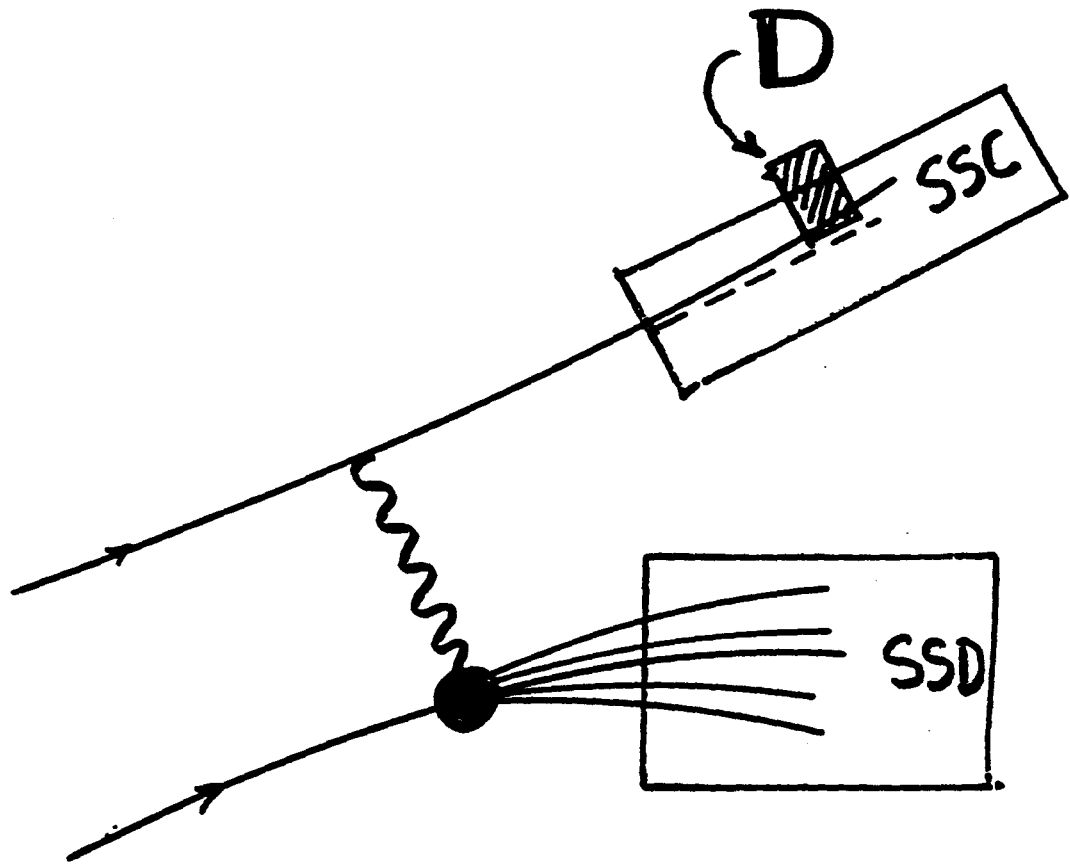
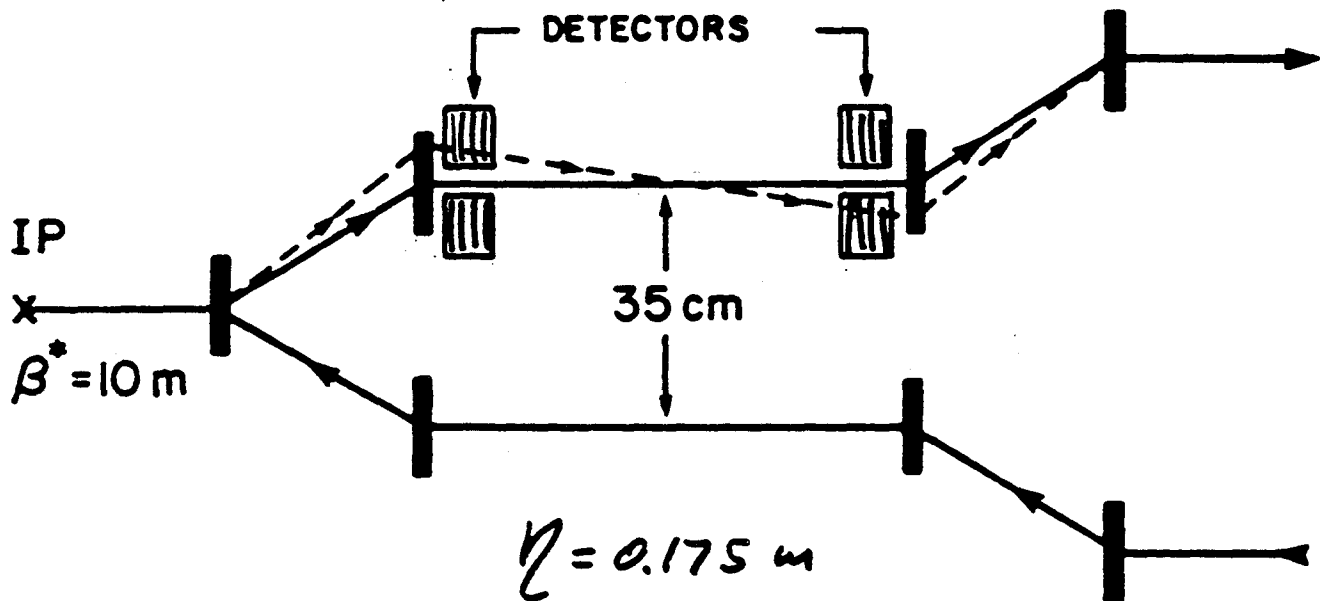


Fig.2: Schematic drawing of the charged particle pseudorapidity distribution of a diffractive cluster of mass M created in a $pp \rightarrow Xp$ collision at \sqrt{s} .

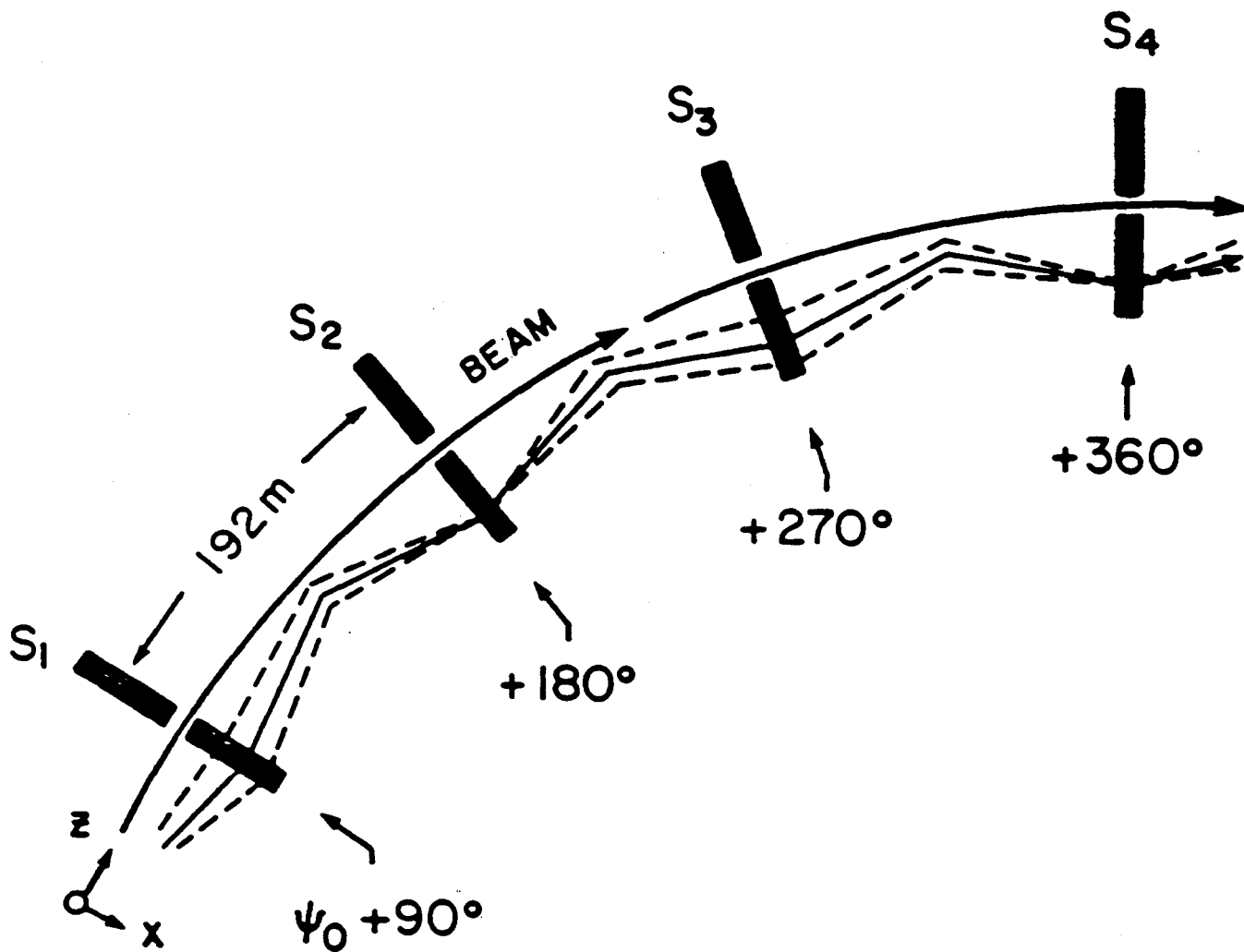


The vertical spectrometer



Distance from beam mm	$\Delta p/p$ (1-x)	Mass M (for t=0) TeV	Mass Resolution dM/M
1	5.7×10^{-3}	3.0	5 %
2.25	1.3×10^{-2}	4.5	2.5 %
5	2.9×10^{-2}	6.8	1.1 %
15	0.09 ←	12	0.4 %

The horizontal spectrometer



Distance from beam mm	$\Delta p/p$ (1-x)	Mass M (for $t=0$) TeV	Mass Resolution dM/M
1	4×10^{-4} ←	0.8	8.3 %
2.5	1×10^{-3}	1.3	3.3 %
15	6×10^{-3}	3.1	0.6 %

$$\Delta x = \eta_x \frac{\Delta P}{P}$$

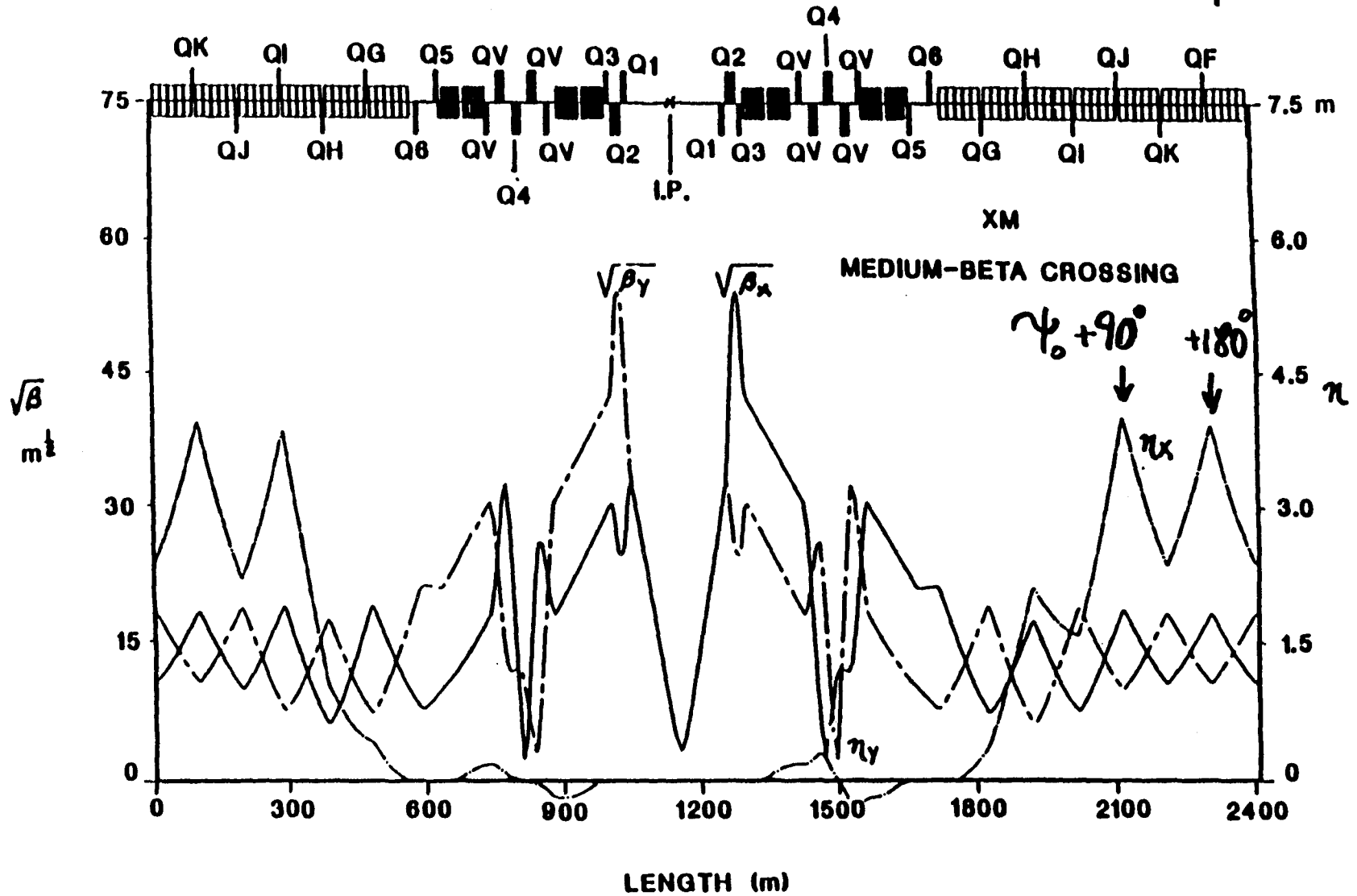


Fig. PL6 Medium-Beta Crossing Lattice Functions

SPECTROMETER PARAMETERS

$$\left\{ \begin{array}{l} \eta_x = 2.5 \text{ m} \\ \beta^* = 10 \text{ m} \\ \beta_x = 250 \text{ m} \\ E = 10^{-6} \text{ m-rad} \end{array} \right.$$

$$\Delta x = \eta_x \frac{\Delta p}{p}$$

$$L_{\text{eff}} = (\beta_x \beta^*)^{1/2}$$

$$50 \text{ m}$$

$$\sigma_x = (\epsilon \beta_x / \gamma)^{1/2}$$

$$100 \text{ f}$$

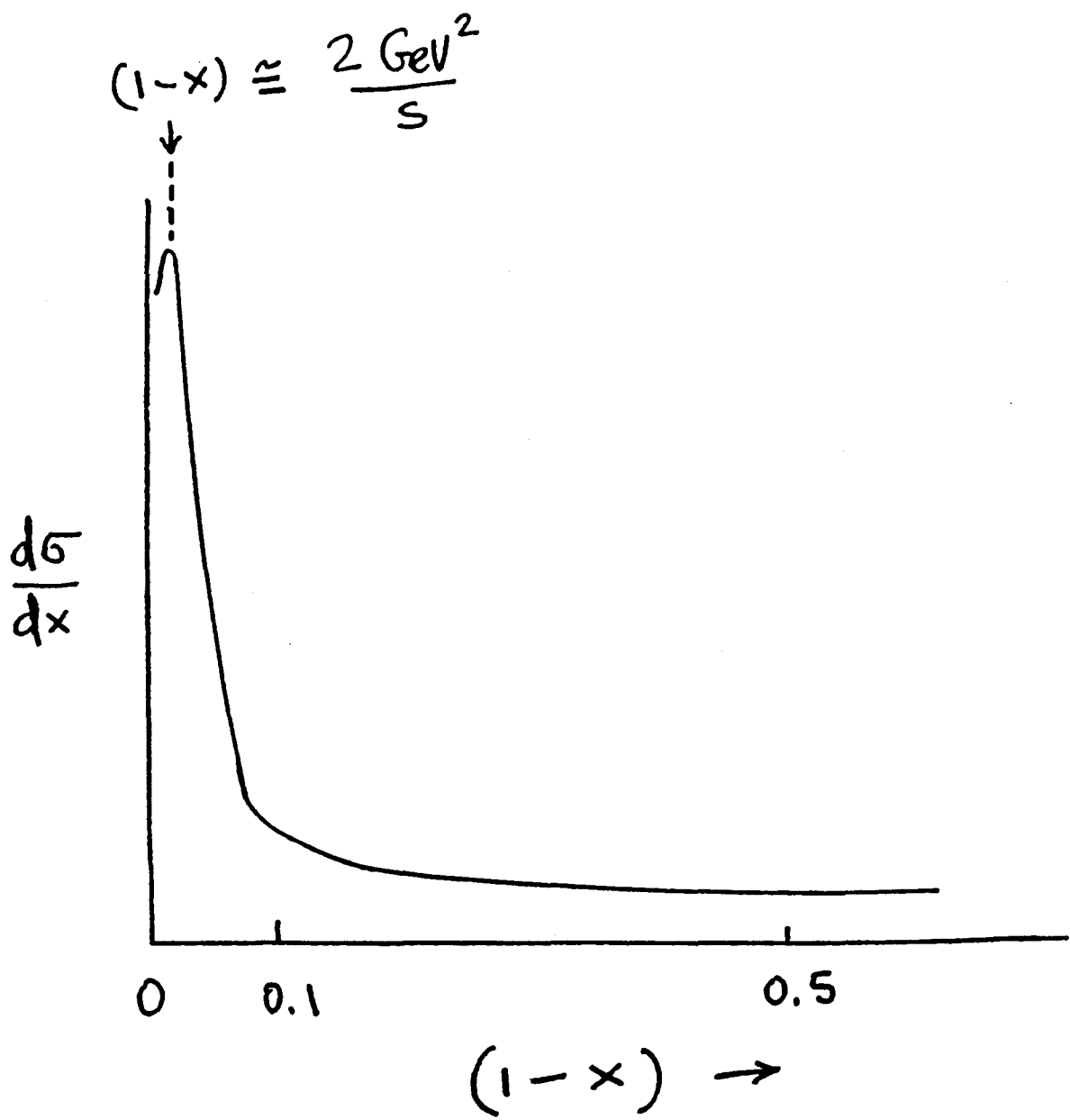
$$|t|_{el} = [(\Delta x_{\text{at } 90^\circ} / L_{\text{eff}}) P_{\text{beam}}]^{1/2}$$

MASS RESOLUTION

$$\frac{M^2}{s} = \frac{\Delta p}{p} \Rightarrow \frac{dM}{M} = \frac{d(\Delta p/p)}{M^2/s} = \frac{1}{2} \frac{d(\Delta p/p)}{1-x}$$

$$(\Delta p/p)_{\text{beam}} = 5 \times 10^{-5}$$

$$d(\Delta p/p)_{\text{position}} \approx \sigma_x / \eta_x \quad 4 \times 10^{-5}$$



$$\frac{d\sigma}{dx} \sim \frac{1}{1-x}$$

SSC: Height of peak $\sim \frac{0.15}{2 \text{ GeV}^2} \approx 10^8 !$

$$\left. \begin{aligned} \frac{d\sigma}{dM^2} &= \frac{A}{M^2} \\ \bar{\eta}_M &= \ln \frac{\sqrt{s}}{M} \end{aligned} \right\} \Rightarrow \frac{d\sigma}{d\bar{\eta}_M} = 2A \approx 1.4 \text{ mb}$$

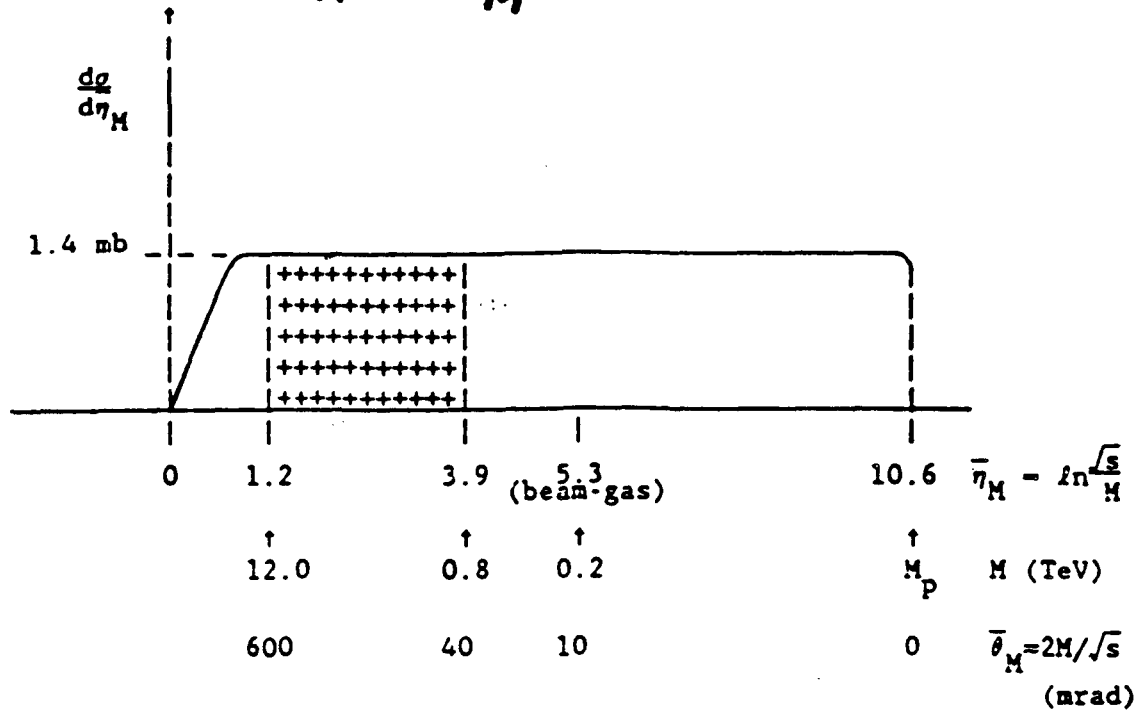


FIG. 4: Single diffraction dissociation cross section $d\sigma/d\bar{\eta}_M$ versus $\bar{\eta}_M$, where $\bar{\eta}_M$ is the average pseudorapidity of a cluster of mass M . The crossed area corresponds to the acceptance of the "diffractive spectrometers".

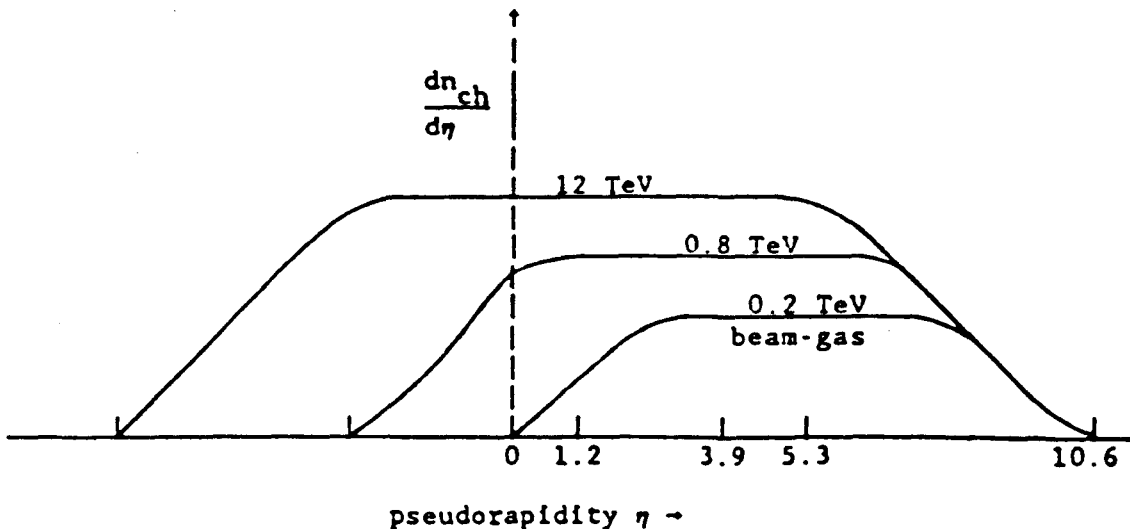


FIG. 5: Charged particle pseudorapidity distribution for various mass values.

HARD DIFFRACTION

Event and Background Rates

$$\beta^* = 10 : \quad L = 5.6 \times 10^{31} / \text{cm}^2 \text{ sec}$$

Single Diff. x-section within acceptance of each spectrometer:

$$-1 \text{ mb} \quad \text{-----} \rightarrow \text{Rate: } \sim 6 \times 10^4 / \text{sec}$$

$$\text{Beab-gas rate: } \sim 3 \times 10^4 / \text{sec}$$

Beam halo from low beta IR: $\sim 10^4 / \text{sec}$
(assuming halo is "killed within a few revolutions)

Occupancy of buckets by background: $\sim \text{a few } 10^4 / (10^9 / 15) \sim 10$